HHS Public Access

Author manuscript

J Hepatol. Author manuscript; available in PMC 2024 July 11.

Published in final edited form as:

J Hepatol. 2023 August ; 79(2): 378–393. doi:10.1016/j.jhep.2023.03.041.

HILPDA promotes NASH-driven HCC development by restraining intracellular fatty acid flux in hypoxia

Davide Povero[1,8,*], **Yongbin Chen**[1], **Scott M. Johnson**[1], **Cailin E. McMahon**[1], **Meixia Pan**[2], **Hanmei Bao**[2], **Xuan-Mai T. Petterson**[3], **Emily Blake**[4], **Kimberly P. Lauer**[4], **Daniel R. O'Brien**[4], **Yue Yu**[4], **Rondell P. Graham**[5], **Timucin Taner**[6], **Xianlin Han**[2,7], **Gina L. Razidlo**[1,8], **Jun Liu**[1,*]

[1]Department of Biochemistry and Molecular Biology, Mayo Clinic, 200 First Street, Rochester, MN 55905, USA

[2]Barshop Institute for Longevity and Aging Studies, University of Texas Health Science Center at San Antonio, 4939 Charles Katz Drive, San Antonio, TX 78229, USA

[3]Metabolomics Core, Mayo Clinic, 200 First Street, Rochester, MN 55905, USA

[4]Department of Quantitative Health Sciences, Mayo Clinic, 200 First Street, Rochester, MN 55905, USA

[5]Department of Laboratory Medicine and Pathology, Division of Anatomic Pathology, Mayo Clinic, 200 First Street, Rochester, MN 55905, USA

[6]Departments of Surgery and Immunology, Mayo Clinic, Rochester, MN 55905, USA

[7]Department of Medicine, Division of Diabetes, University of Texas Health Science Center at San Antonio, San Antonio, TX 78229, USA

[8]Department of Gastroenterology and Hepatology, Mayo Clinic, Rochester, MN 55905, USA

Abstract

Background & Aims: The prevalence of non-alcoholic steatohepatitis (NASH)-driven hepatocellular carcinoma (HCC) is rising rapidly, yet its underlying mechanisms remain unclear. Herein, we aim to determine the role of hypoxia-inducible lipid droplet associated protein (HILPDA)/hypoxia-inducible gene 2 (HIG2), a selective inhibitor of intracellular lipolysis, in NASH-driven HCC.

[*]Corresponding authors. Address: Department of Biochemistry and Molecular Biology, Mayo Clinic, 200 First Street SW, Rochester, MN 55905, USA; liu.jun@mayo.edu (J. Liu), povero.davide@mayo.edu (D. Povero).

Authors' contributions

Conceived the idea: DP, JL. Designed the experiments: DP. Performed the experiments: DP, YC, SMJ, CEM, HB, MP, XTP. Analyzed the data: DP, YY, EB, KPL, RPG, XTP, DRO, NCM. Contributed human specimens: TT. Contributed reagents/materials/analysis tools: DP, HB, MP, XTP, YY, EB, KPL, DRO, NCM. Wrote/revised the manuscript: DP, JL. Reviewed/edited the manuscript: DP, JL, GLR, XH. All authors discussed and commented on the manuscript.

Conflict of interest

The authors declare no conflicts of interest that pertain to this work.

Please refer to the accompanying ICMJE disclosure forms for further details.

Supplementary data

Supplementary data to this article can be found online at https://doi.org/10.1016/j.jhep.2023.03.041.

Methods: The clinical significance of HILPDA was assessed in human NASH-driven HCC specimens by immunohistochemistry and transcriptomics analyses. The oncogenic effect of HILPDA was assessed in human HCC cells and in 3D epithelial spheroids upon exposure to free fatty acids and either normoxia or hypoxia. Lipidomics profiling of wild-type and *HILPDA* knockout HCC cells was assessed via shotgun and targeted approaches. Wild-type (*Hilpda*$^{fl/fl}$) and hepatocyte-specific *Hilpda* knockout (*Hilpda*$^{\Delta Hep}$) mice were fed a Western diet and high sugar in drinking water while receiving carbon tetrachloride to induce NASH-driven HCC.

Results: In patients with NASH-driven HCC, upregulated HILPDA expression is strongly associated with poor survival. In oxygen-deprived and lipid-loaded culture conditions, HILPDA promotes viability of human hepatoma cells and growth of 3D epithelial spheroids. Lack of HILPDA triggered flux of polyunsaturated fatty acids to membrane phospholipids and of saturated fatty acids to ceramide synthesis, exacerbating lipid peroxidation and apoptosis in hypoxia. The apoptosis induced by HILPDA deficiency was reversed by pharmacological inhibition of ceramide synthesis. In our experimental mouse model of NASH-driven HCC, *Hilpda*$^{\Delta Hep}$ exhibited reduced hepatic steatosis and tumorigenesis but increased oxidative stress in the liver. Single-cell analysis supports a dual role of hepatic HILPDA in protecting HCC cells and facilitating the establishment of a pro-tumorigenic immune microenvironment in NASH.

Conclusions: Hepatic HILPDA is a pivotal oncometabolic factor in the NASH liver microenvironment and represents a potential novel therapeutic target.

Graphical abstract

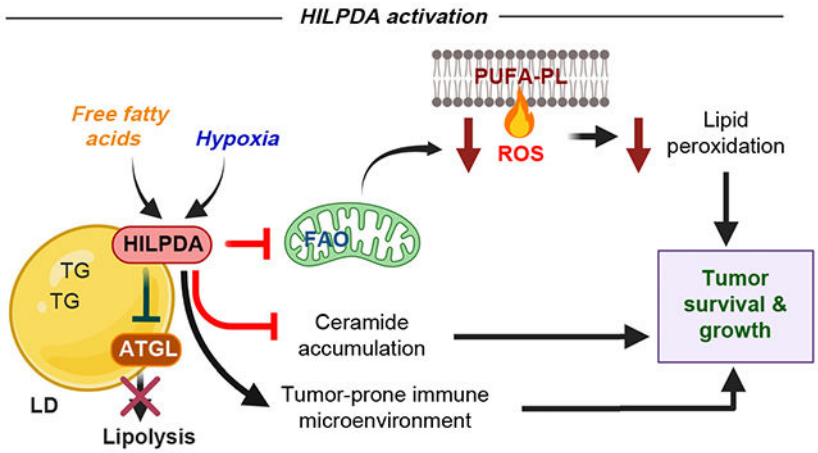

Keywords

Nonalcoholic steatohepatitis; Hepatocellular carcinoma; lipid metabolism; Hypoxia; HILPDA; lipidomics

Introduction

Non-alcoholic fatty liver disease (NAFLD) is one of the most common chronic liver diseases, with a global prevalence of approximately 25% that is continuing to rise rapidly.[1,2] NAFLD is driven by obesity, insulin resistance and hyperlipidemia. At early stages it is

characterized by simple liver steatosis which has a more benign course.[2] However, NAFLD frequently progresses to non-alcoholic steatohepatitis (NASH), which is characterized by persistent liver inflammation, liver injury, fibrosis and eventual cirrhosis.[3,4] Mounting epidemiological evidence also indicates NASH as a leading cause of hepatocellular carcinoma (HCC), the most common form of liver cancer[5,6] and third-leading cause of cancer-related deaths worldwide.[7] Compared to other etiologies, NASH-driven HCC displays a significant enrichment of molecular signatures associated with oxidative stress and lipid metabolism.[8] Despite immense efforts to target a variety of disease pathways over the years, no effective therapies are currently available for either NASH or NASH-driven HCC.

Tumor tissues are chronically exposed to low oxygen (hypoxia) owing to aberrant vascularity and rapid growth of tumor cells away from blood vessels. In various solid tumors, including HCC, hypoxia induces metabolic alterations, thereby promoting aggressive carcinogenesis, tumor invasiveness and poor survival, as well as resistance to chemotherapy.[9–11] The hypoxia responsive pathway operates as a metabolic checkpoint by sensing low oxygen availability and through stabilizing hypoxia inducible factors (HIFs). Upon nuclear translocation, HIF-1 and -2 activate the expression of a multitude of genes and their encoded proteins, which act coordinately to maintain oxygen and redox homeostasis and thereby alleviate hypoxic stress.[11–15] While previous efforts largely focused on adaptive responses mediated by HIFs in glucose and glutamine metabolism, recent studies have begun to yield important insight into the hypoxic regulation of lipid metabolic reprogramming in cancer.[16]

Emerging evidence points to triglyceride lipid droplet (TG-LD) accumulation as a hallmark of hypoxic cancer cells.[17] In this regard, our group previously identified hypoxia-inducible lipid droplet associated protein (HILPDA, also known as HIG2) as a selective endogenous inhibitor of adipose triglycerides lipase (ATGL), the rate-limiting enzyme for intracellular triglyceride (TG) hydrolysis or lipolysis.[16,18] Although other lipolysis-independent roles were suggested for HILPDA,[19,20] evidence obtained from various cell types strongly indicates that ATGL inhibition is the major mechanism underlying the TG-promoting effect of HILPDA.[18,21–23] In response to hypoxia, *HILPDA* mRNA expression is activated upon HIF-1 binding to the functional hypoxia response elements in its promoter.[24] In colorectal and renal cancer cells, upregulated HILPDA expression promotes TG-LD accumulation, attenuates fatty acid (FA) oxidation and reactive oxygen species (ROS) generation, and thereby enhances cell survival in hypoxia.[18] Xenografted tumors derived from Hilpda-deficient colon cancer cells exhibited impaired growth and increased apoptosis in immunodeficient mice.[18,21] However, to date, the functional relevance of HILPDA in endogenous tumor development has not been established using genetically engineered mouse models, where the influence of the tissue microenvironment is more properly maintained.

HCC is recognized as one of the most hypoxic tumors, with median oxygen levels as low as 0.8%.[25] Yet, the basic mechanisms underlying the hypoxic regulation of HCC metabolism are not fully understood. Even less is known about how HCC initiation and progression react to hypoxia in the lipid-rich NASH microenvironment and whether these processes involve

HILPDA in hepatocytes. In mice, the liver normally expresses low levels of HILPDA. Hepatocyte-specific Hilpda deletion elicited no significant impact on lipid and energy metabolism except for a moderately increased rate of hepatic TG turnover.[26] Although treatment with a methionine- and choline-deficient diet increased HILPDA expression in the liver, HILPDA deletion only led to a modest decrease in hepatic TG content without noticeable changes in classical NASH-like features, including ballooning, inflammation, steatosis, and fibrosis.[19] Despite these previous efforts to explore its liver-specific role, the effects of HILPDA on the development of NASH-driven HCC, a setting with more severe hypoxia, remained undetermined. During the development of NASH, accumulation of lipids and other lipid-derivatives in the liver affects both hepatocytes and non-parenchymal hepatic and extrahepatic cells including diverse types of immune cells. Damaged hepatocytes are known to evoke immune responses by releasing various signals to activate resident and recruited immune cells. Given the role of HILPDA in regulating intracellular lipid flux and oxidative stress, it is also worth asking whether HILPDA in hepatocytes plays a role in reshaping the hepatic immune microenvironment in NASH. In this regard, enrichment of NASH-associated macrophages (NAMs) and T-cell exhaustion are thought to signify a tumor-prone microenvironment in NASH.[27–29]

In the current study, we examined the expression of HILPDA in human NASH-driven HCC and investigated the metabolic role of HILPDA in established HCC cell lines as well as in 3D epithelial spheroids upon their exposure to hypoxia and exogenous free FAs. We also examined the impact of hepatocyte-specific Hilpda deletion in an experimental mouse model of NASH-driven HCC. Our results provide novel insights into the mechanisms underlying HILPDA's action in protecting HCC cells from hypoxia and lipotoxicity as well as promoting tumorigenesis in NASH.

Materials and methods

Study design

This study was designed to investigate the oncometabolic function of HILPDA in NASH-driven HCC and to assess the effects of HILPDA loss-of-function *in vitro* and in a pre-clinical mouse model. The clinical impact of HILPDA was assessed in human HCC and NASH-driven HCC cohorts. All human sample collection and study protocols were approved by the Mayo Clinic Institutional Review Board (IRB) under protocol number 21-009176. The metabolic function of HILPDA was assessed *in vitro* using hepatoma and HCC cell lines exposed to free FA-enriched culture media. *In vitro* HCC models included both 2D cells and 3D epithelial spheroids. For *in vivo* studies, wild-type and hepatocyte-specific *Hilpda* knockout mice were fed a Western diet plus sugar in water and were injected with CCl_4 weekly for 24 weeks to investigate the oncogenic role of Hilpda during NASH-driven HCC tumorigenesis. For *in vitro* studies, three experiments were performed in triplicates or more. For *Hilpda* knockout *in vivo* studies, 14 male mice were randomly assigned to the two experimental groups. *In vitro* and *in vivo* experiments were not blinded. For further details regarding the materials and methods used, please refer to the supplementary information.

Statistical analysis

All statistical tests were performed using GraphPad Software v9.5.1. Data are presented as means ± SD of three or more replicates. Data reported was replicated in three independent experiments. Overall survival in relation to expression was evaluated by the Kaplan-Meier survival curve and the log-rank test. Differences between three or more groups were compared by a non-parametric Kruskal-Wallis ANOVA test. If a significant effect was detected, *post hoc* pair-wise comparisons were performed using Mann-Whitney tests with Bonferroni correction. Differences between two groups were compared by a two-sided Student's *t* test if the data were normally distributed or a Mann-Whitney *U* test if the data deviated from the normal distribution. Differences were considered to be statistically significant at *p* values of <0.05.

Results

HILPDA expression is upregulated and associated with poor prognosis in human HCC

To determine the clinical significance and prognostic value of HILPDA in human HCC, we first analyzed the mRNA expression of *HILPDA* using TCGA (The Cancer Genome Atlas datasets. Our results show that expression of HILPDA was significantly upregulated in HCC tissues compared to adjacent non-cancerous tissues (Fig. 1A). The Kaplan-Meier survival analysis revealed that expression level of HILPDA is inversely associated with survival probability in humans with HCC (p =2.12e-07; Fig. 1B). Given that HILPDA is upregulated during hypoxic conditions, we investigated whether the mRNA expression of *HILPDA* correlates with the level of intratumor hypoxia (modest or severe). We defined the hypoxia score by extracting the normalized expression values for human hypoxia response genes using Gene Ontology (n = 330). Specifically, a score of +1 was assigned to all samples with the top 50% expression and −1 to all the samples with the bottom 50% expression, with all the scores summed for each sample. Overall, severe intratumoral hypoxia was more positively associated with upregulation of *HILPDA* mRNA compared to the modest level of intratumoral hypoxia (Fig. 1C). This result indicates that like in other types of solid tumors, intratumoral hypoxia also enhances HILPDA expression in HCC.

Because HILPDA can be induced by exogenous free FAs, in addition to hypoxic conditions, and promotes accumulation of intracellular TGs in LDs,[18,19] we sought to investigate the oncometabolic role of HILPDA in NASH-driven HCC, which develops in a highly hypoxic and lipid-rich environment.[30,31] First, we performed a spatial transcriptomics analysis in a patient with histopathologically proven NASH-driven HCC and adjacent non-cancerous tissue, which demonstrated that *HILPDA* mRNA expression mostly co-localized with the steatohepatitic HCC marker glutamine synthetase and hypoxia-inducible factor 1α within the NASH-driven HCC tissue sample (Fig. 1D). Secondly, using immunohistochemistry and quantitative real-time PCR, we further examined HILPDA expression in NASH-driven HCC, adjacent non-cancerous tissue and normal liver samples. The clinicopathological features of the patients included in the study are shown in Table 1. Immunohistochemical staining showed that while it was at a low level in normal liver tissue (Case 1, Fig. 1E), HILPDA was particularly circumscribed in tumor compared to adjacent non-cancerous tissues (Cases 2 & 3, Fig. 1E). Relative to that in Case 3, HCC in Case 2 exhibited higher level of HILPDA

along with an increase in both the size and number of intratumoral fat vacuoles that resemble lipid droplets (LDs). Moreover, quantitative reverse-transcription PCR analysis confirmed a significant upregulation of HILPDA expression in HCC compared to adjacent non-cancerous tissue (Fig. 1F). Taken together, these findings suggest that HILPDA, whose expression is strongly associated with poor prognosis and survival, is likewise upregulated in NASH-driven HCC.

HILPDA promotes cell growth and inhibits cell death in HCC cell lines under hypoxic and FA-rich conditions

HIF-1 was previously shown to mediate *HILPDA* mRNA transcription in hypoxia.[24] More recently, it was reported that upregulation of HILPDA can occur post-transcriptionally upon free FA treatment.[21] We determined HILPDA protein expression in three human HCC or hepatoma cell lines (Huh7, HepG2 and Hep3B) upon exposure to normoxia or hypoxia and treatment with or without FAs. While HILDPA was upregulated in HepG2 and Hep3B cells exposed to hypoxia and FAs (Fig. S1A,B), Huh7 cells responded better to FAs and hypoxia by upregulating HILPDA (Fig. 2A) and are more suitable for 3D cultures. To determine how conditions mimicking the microenvironment of NASH-driven HCC would impact HILPDA expression, we treated Huh7 hepatoma cells with or without various free FAs including oleate, palmitate and linoleate under either normoxic or hypoxic conditions. Hypoxia and FA treatment increased HILPDA protein expression in Huh7 cells both singly and additively (Fig. 2A). The additive effects of hypoxia and FAs were most notable when hypoxic cells were treated with linoleic acid or oleic acid (Fig. 2A). In addition, immunofluorescence staining revealed a specific localization of HILPDA to the surface of LDs in hypoxic Huh7 cells treated with oleic acid (Fig. 2B).

To assess the oncogenic effect of HILPDA in human hepatoma cells, we knocked out HILPDA in Huh7 and Hep3B cells using CRISPR/Cas9. No effects of HILPDA deletion were observed on ATGL expression (Fig. 2C, Fig. S1B). Hypoxia induced the formation of numerous and large LDs as well as the accumulation of TGs in wild-type cells. However, in HILPDA knockout (HILPDA KO) cells, the amounts of intracellular LDs and TGs were dramatically reduced under both normoxic and hypoxic conditions (Fig. 2D,E). Functional characterization revealed that HILPDA deletion significantly reduced the viable cell numbers when Huh7 and Hep3B cells were cultured in normoxic or hypoxic conditions (Fig. 2F,G, Fig. S1C). Compared to the slight decrease in normoxic and hypoxic cell proliferation (Fig. 2H), intracellular caspase 3/7 activity was enhanced by 50% in hypoxic HILPDA KO cells treated with the FA mix (Fig. 2I). These results suggest that HILPDA mostly acts to sustain HCC cell survival by protecting against metabolic stress-induced apoptosis under hypoxia.

Deletion of HILPDA disrupts lipid homeostasis and increases PUFA-enrichment in membrane phospholipids

To uncover the mechanisms underlying lipid-induced cell death, we performed a lipidomics analysis to examine whether HILPDA knockdown resulted in derangement of lipid homeostasis. As shown in Fig. 3A,G, hypoxic treatment upregulated total TG synthesis as well as enrichment of linoleic acid (C18:2) in TG in the wild-type Huh7 cells. On

the contrary, in HILPDA KO Huh7 cells exposed to hypoxia, linoleic acid enrichment in TG was downregulated by 50% compared to wild-type hypoxic cells (Fig. 3A,G). Upon further investigation, we found that polyunsaturated FA (PUFA)-enriched cardiolipins and membrane phospholipids, including phosphatidylethanolamine (PE), phosphatidylserine, phosphatidylglycerol and lysophosphatidylethanolamine (LPE) but not phosphatidylcholine, were upregulated in hypoxic HILPDA KO Huh7 cells compared to wild-type cells (Fig. 3A). Strikingly under hypoxia, the membrane phospholipids in HILPDA KO Huh7 cells exhibited enrichments of PUFA moieties, particularly C18:2, C18:3 and C20:4, compared to wild-type cells (Fig. 3B–F). A recent study suggested that HILPDA promotes enrichment of PUFAs in both TGs and phospholipids in clear-cell carcinoma.[32] To directly determine whether HILPDA controls PUFA flux from LDs to membrane phospholipids, we treated wild-type control and HILPDA knockdown Huh7 cells with ^{14}C-labeled linoleic acid (^{14}C-LA) under normoxic and hypoxic conditions. Thin-layer chromatography analysis showed that while hypoxia promoted ^{14}C-LA enrichment in TGs in the control cells, such an enrichment was significantly decreased upon HILPDA knockdown (Fig. 3H). Concomitantly, we observed a marked increase of ^{14}C-LA incorporation into PE and to a lesser extent into phosphatidylcholine, the two most abundant membrane phospholipids, in the hypoxic HILPDA knockdown cells (Fig. 3I,J). These findings seem to point to a role of HILPDA as a metabolic checkpoint which promotes the sequestration of PUFAs in TG-LDs away from membrane phospholipids.

HILPDA deficiency disrupts sphingolipid homeostasis, leading to caspase 3-dependent apoptosis of hepatoma cells

Resistance to mitochondrial apoptosis is a prominent feature of cancer cells. However, in some cases, ceramides can override such resistance, leading to cancer cell apoptosis.[33,34] Strikingly, as revealed by our unbiased lipidomics analysis, total ceramide levels increased substantially in hypoxic HILPDA KO Huh7 cells compared to wild-type cells (Fig. 4A). Specifically, we observed a significant accumulation of various major species of ceramides including C16-, C18- and C24-ceramides (Fig. 4B) and parallel reduction of serine levels, suggesting a greater consumption of serine via *de novo* ceramide synthesis by the hypoxic HILPDA KO cells (Fig. S2A). In comparison, HILPDA deletion did not seem to affect the low ceramide levels in normoxic cells. These findings were largely corroborated by a targeted lipidomics analysis when HILPDA in Huh7 cells was transiently knocked down using small-interfering RNA (Fig. 4C,D). Increased ceramide accumulation in HILPDA knockdown cells was accompanied by increased accumulation of other sphingolipids such as sphingosine-1-phosphate, sphingosine and sphinganine (Fig. 4E). Consistently, in HILPDA-depleted cells under hypoxia, we observed upregulation of palmitoyltransferase long chain base subunit 1 (*SPTLC1*), the rate-limiting enzyme of the *de novo* ceramide synthesis pathway, and of ceramide synthase 2 (*CERS2*) and 6 (*CERS6*), two enzymes involved in the synthesis of long acyl chain ceramides in the ceramide salvage pathway (Fig. 4F). Furthermore, while no effects were observed in normoxic cells, HILPDA deletion led to a marked increase in intracellular caspase-3/7 activity in hypoxic cells. Importantly, this increase in caspase-3/7 activity was significantly reversed after hypoxic HILPDA KO cells were treated with either fumonisin B1 or Myriocin (Fig. 4G,H), two pharmacological inhibitors of ceramide synthesis. As expected, treatment with fumonisin B1 or myriocin led

to a drastic reduction in various ceramide species in the hypoxic HILPDA KO cells (Fig. S2B). Taken together, these results suggest that increased ceramide synthesis is involved in the apoptotic induction caused by the loss of HILPDA.

HILPDA deletion exacerbates intracellular oxidative stress, membrane phospholipid peroxidation and mitochondrial damage

In the absence of HILPDA, ATGL-mediated lipolysis is uninhibited, leading to increased channeling of FAs into the mitochondrial oxidative pathway and overproduction of ROS under hypoxia.[18] Under oxidative stress, high PUFA content renders cellular membranes more susceptible to lipid peroxidation.[35] Indeed, we observed increased ROS production (Fig. 5A,B) and more pronounced lipid peroxidation (Fig. 5C,D) in HILPDA KO cells than wild-type controls when cells were treated with the FA mix under hypoxia. Hypoxic HILPDA KO cells were particularly susceptible to membrane lipid peroxidation following treatment with linoleic acid, compared to exposure to palmitic and oleic acids (Fig. S3A,B). Increased lipid peroxidation in the HILPDA KO cells was further confirmed by increased level of malondialdehyde, the final product of intracellular PUFA peroxidation (Fig. 5E). In addition, hypoxic HILPDA KO cells exposed to FAs displayed a significant decrease of mitochondrial membrane potential as revealed by MitoTracker CMXRos staining (Fig. 5F,G). Under the same conditions, the expression of mitochondrial promoter of metabolic stress-induced cell death, long-chain acyl-CoA synthetase 5 (*ACSL5*),[36] was significantly upregulated in the HILPDA KO cells compared to the control cells (Fig. 5H). Taken together, these findings suggest that by sequestering PUFAs in TG-LDs away from membrane phospholipids, HILPDA prevents lipid peroxidation and reduces oxidative damage in Huh7 cells under hypoxic and lipid-rich conditions. This occurs in parallel to HILPDA's reported role as an inhibitor of ATGL-mediated lipolysis, FA oxidation and ROS production.

HILPDA depletion impairs anchorage-independent growth and survival of hepatoma epithelial spheroids

Simple 2D culture models of liver cancer are associated with limitations, including the lack of a cellular microenvironment, proper cell-cell communication, and 3D tumor structure. To address these limitations, we generated 3D epithelial spheroids using Huh7 cells (Fig. 6A), which exhibited a progressive spheroid anchorage-independent growth over a 6-day period (Fig. 6B) and remained viable for up to 2 weeks in culture. Morphologically, the Huh7 spheroids were capable of reaching ~400 μm in diameter and displayed liver tissue-like architecture, including the presence of intracellular LDs (Fig. 6C). To better mimic the lipid-rich tumor microenvironment, we incubated Huh7 spheroids with palmitic:oleic:linoleic acid-enriched medium. Reminiscent of what was often observed in solid tumors, Huh7 3D spheroids naturally developed heterogenous core regions of hypoxia and LD accumulation (Fig. 6D,E). Interestingly, when compared to the wild-type spheroids which exhibit a HILPDA-enriched central core, HILPDA KO spheroids were significantly smaller in size (Fig. 6F–H). Their anchorage-independent growth was markedly impaired as early as after 1 day in culture and more dramatically after 6 days in culture (Fig. 6I,J). HILPDA KO spheroids only showed a slight decrease of proliferation in comparison to the wild-type controls (Fig. 6K), suggesting that the

difference in spheroid size is attributable to the ability of HILPDA to sustain cell survival in this lipid-rich, 3D culture setting. Moreover, transmission electron microscopy[23] analysis revealed severe mitochondrial structural damage in HILPDA KO spheroids, as indicated by mitochondria fragmentation, rupture of mitochondrial membrane and enlargement of mitochondrial cristae (Fig. 6L). Immunoblotting analysis further showed an upregulated expression of pro-caspase-8 (57 kDa), cleaved caspase-8 (43/41 kDa), pro-caspase-3 (35 kDa) and cleaved caspase-3 (17 kDa) in the HILPDA KO spheroids when compared to the wild-type controls (Fig. 6M). Collectively and consistently with our 2D cell culture data, these findings suggest that HILPDA deletion impairs Huh7 spheroid survival and anchorage-independent growth, presumably as a consequence of mitochondrial damage and metabolic stress-induced apoptosis.

Hepatocyte-specific Hilpda knockout ameliorates NAFLD activity score while leading to increased hepatic oxidative stress in mice

To determine the relevance of Hilpda knockout in NASH development *in vivo*, we generated unique hepatocyte-specific *Hilpda* knockout (Hilpda$^{\Delta Hep}$) mice by crossing *Hilpda*-floxed (Hilpda$^{fl/fl}$) mice to an established albumin-Cre driver (Fig. S4A). To evaluate the role of Hilpda in experimental NASH, we treated *Hilpda*$^{\Delta Hep}$ mice with a Western diet, plus fructose and glucose in drinking water, combined with a weekly injection of the hepatotoxin carbon tetrachloride (CCl_4) for 24 weeks (Fig. S4B), as previously described.[37] *Hilpda*$^{fl/fl}$ mice were used as the wild-type controls. Longitudinal and terminal body weight measurements showed no changes between the two groups (Fig. S4C,D). However, *Hilpda*$^{\Delta Hep}$ mice displayed a significant reduction of liver weight (Fig. 7A) and liver/body weight ratio (Fig. 7B) in comparison to the control animals. Further, the smaller liver mass observed in *Hilpda*$^{\Delta Hep}$ mice was associated with significantly decreased hepatic TG levels (Fig. 7C). A blind histopathological assessment of liver tissues revealed that *Hilpda*$^{\Delta Hep}$ mice developed less liver steatosis and ballooning than control *Hilpda*$^{fl/fl}$ animals. However, the two groups showed no difference in lobular inflammation (Fig. 7E). Fibrosis was slightly but not significantly reduced in *Hilpda*$^{\Delta Hep}$ livers (Fig. 7F). While *Hilpda* mRNA expression was reduced in both dysplastic nodules and adjacent parenchyma in the *Hilpda*$^{\Delta Hep}$ liver (Fig. S4E), expression of pro-inflammatory markers (*Il1β*, *Il6*, *Ifnγ*) and the pro-fibrogenic marker *Col1α1* remained unchanged between the two groups, with the exception of *Tnfα* which was upregulated in *Hilpda*$^{\Delta Hep}$ adjacent liver parenchyma but not in dysplastic nodules (Fig. S4G). Overall, *Hilpda*$^{\Delta Hep}$ mice displayed lower NAFLD activity scores (Fig. 7D,E). In addition to reduced macrovesicular and microvesicular steatosis (Fig. 7G, H&E), Hilpda deletion in hepatocytes resulted in increased accumulation of iron oxidation products, as demonstrated by Prussian blue staining (Fig. 7G), and increased oxidative stress, as outlined by immunohistochemistry for the oxidative stress marker 8-hydroxyguanosine (Fig. 7G,H). Despite these histological changes, Hilpda deletion did not appear to affect plasma liver injury markers (Table S3) and plasma TG (Fig. S4F). Nonetheless, these findings as a whole suggest that hepatocyte-specific Hilpda deletion ameliorates hepatic steatosis and ballooning while increasing the overall oxidative stress in the liver of mice fed with the NASH-inducing diet.

Hepatocyte-specific Hilpda knockout delays NASH-driven HCC formation in mice

To further evaluate the role of Hilpda in liver tumorigenesis, we examined NASH-driven HCC formation in *Hilpda*$^{\Delta Hep}$ and *Hilpda*$^{fl/fl}$ control mice. Gross examination of isolated liver showed that *Hilpda*$^{\Delta Hep}$ mice developed ~3-fold fewer nodules than control mice (Fig. 7I,J). Based on histopathological assessment, the tumors were diagnosed as dysplastic nodules[39] with steatohepatitic features (Fig. 7K). Expression of glypican-3 (*Gpc3*), a widely established marker of HCC, was considerably higher in nodules resected from the wild-type control livers than those resected from the *Hilpda*$^{\Delta Hep}$ livers (Fig. 7L). In comparison to the wild-type controls, *Hilpda*$^{\Delta Hep}$ nodules exhibited upregulation of tumor-suppressor and intracellular iron storage promoter ferritin heavy chain (*Fth1*), downregulation of *de novo* lipogenesis enzyme FA synthase (*Fasn*), and upregulation of FA oxidation enzyme carnitine O-palmitoyltransferase 1 (*Cpt1*) (Fig. 7L). *Hilpda*$^{\Delta Hep}$ livers and dysplastic nodules were also associated with downregulation of the HCC cell survival and viability marker octamer-binding transcription factor 4 (*Oct4*)[40] and the cancer stemness marker *Sox2*[41] (Fig. 7L). Furthermore, a targeted lipidomics analysis found that various ceramides including C14-, C16-, C18:1-ceramides as well as sphingosine-1-phosphate trended higher in *Hilpda*$^{\Delta Hep}$ dysplastic nodules than in control *Hilpda*$^{fl/fl}$ dysplastic nodules (Fig. S4H–L), though the differences did not reach statistical significance. Nevertheless, to a great extent, these findings corroborate our results obtained from cell studies, showing that Hilpda depletion enhances FA oxidation and ROS-induced oxidative stress, resulting in impaired cancer cell survival and reduced HCC tumor formation. To further investigate the role of Hilpda in shaping the NASH-driven HCC immune microenvironment, we performed a single-cell RNA-sequencing analysis of *Hilpda*$^{fl/fl}$ and *Hilpda*$^{\Delta Hep}$ livers. Uniform manifold approximation and projection dimensionality reduction analysis identified nine clusters corresponding to the main cell types of mouse liver, including hepatocytes, hepatic stellate cells, Kupffer cells, endothelial cells, T cells, B cells and cholangiocytes in addition to two model-specific clusters: NAMs expressing unique molecular markers (Apoe, Trem2 and C1qa) and dysplastic cells (Fig. 7M). Compared to *Hilpda*$^{fl/fl}$ livers, *Hilpda*$^{\Delta Hep}$ livers exhibited a lower total cell count and lower relative amount of Kupffer cells, NAMs and cancer cells (Fig. 7N). NAMs were reported to progressively increase during tumor formation in NASH and to promote an immunosuppressive liver microenvironment,[27] yet our data shows that their abundance is significantly reduced upon Hilpda depletion.

Despite no difference in T cell numbers between the two animal groups, mRNA expression of genes involved in TCR signaling (*Cd3g, Lck*) and cytokine response (*Ccl5, Tnfrsf18*) were significantly downregulated in T cells from *Hilpda*$^{\Delta Hep}$ mice, reflecting an intermittent rather than a persistent stimulation of T-cell signaling that leads to T-cell exhaustion (Fig. 7O). Consistently, genes known to be involved in T-cell exhaustion, including *Pdcd1* and *Tox*, were significantly downregulated in T cells from *Hilpda*$^{\Delta Hep}$ mice (Fig. 7O). In contrast, mRNA levels of T cell stimulatory factors (*Cd44, Tsc22d3, Cd53*) were significantly upregulated in *Hilpda*$^{\Delta Hep}$ livers compared to *Hilpda*$^{fl/fl}$ livers (Fig. 7O). In addition, T cells isolated from the *Hilpda*$^{\Delta Hep}$ livers showed a significant enrichment of pathways associated with T cell activation (PI3K_AKT_MTOR, IL6_JAK_STAT, IL2_STAT5) and T cell effector functions (IFNγ response, complement, inflammatory response) (Fig. S5A). An unbiased metabolomics analysis revealed that three metabolic

pathways associated with antitumor effector T cells were enriched in *Hilpda*$^{\Delta hep}$ compared to *Hilpda*$^{fl/fl}$ livers (Fig. S5B,C). Furthermore, dysplastic cells isolated from *Hilpda*$^{\Delta Hep}$ livers exhibited upregulation of common tumor suppressor genes (*Stat3, Pten, Tsc2, Axin1, Arid1a, ApoB, Cdk8*), compared to those isolated from *Hilpda*$^{fl/fl}$ livers. Concurrently, mRNA median expression of common oncogenes (*Ctnnb1, Nfe2l2, Rps6ka3, Wnt2*) was downregulated in dysplastic cells from Hilpda-depleted livers compared to those isolated from control livers (Fig. S4M). Pathways associated with ferroptosis, iron homeostasis and oxidative stress response appeared to be enriched in dysplastic cells from *Hilpda*$^{\Delta Hep}$ livers (Fig. S4N). Taken together, these findings indicate that metabolic remodeling mediated by HILPDA in hepatocytes indirectly facilitates the creation of a pro-tumorigenic immune microenvironment in the NASH liver.

Discussion

Development of HCC in the context of NASH is a complex and gradual process that encompasses both oncogenic activity and acquisition of unique metabolic features.[5,6] In this context, the current study provides compelling evidence that HILPDA, whose expression peaks under hypoxic and lipid-rich conditions, is an important switch at the crossroads of lipid metabolism and hepatotumorigenesis. We show that HILPDA mRNA and protein levels are upregulated in cancerous compared to non-cancerous tissues in human NASH-driven HCC. By using HCC cell lines and 3D epithelial spheroids, we demonstrate that by promoting FA storage in TG-LDs, HILPDA plays a key role in preventing lipolysis-derived FAs from entering several downstream metabolic pathways, products of which otherwise would aggravate hypoxic and oxidative stress, lipotoxicity, and apoptosis. In mice where NASH-related HCC was induced via treatment with a Western diet and CCl_4, hepatocyte-specific deletion of Hilpda led to a significant decrease in dysplastic nodule number while reshaping the liver towards a less tumor-prone immune microenvironment. Prior to this study, the *in vivo* relevance of HILPDA was investigated only in xenografted tumors derived from colon cancer cell lines. To the best of our knowledge, the current study represents the first ever effort to establish the pathophysiological relevance of HILPDA in endogenous tumor development using a preclinical experimental mouse model.

The function of HILPDA as a lipolytic inhibitor has been widely described by our group and others.[18,21–23] By physically interacting with ATGL at the LD surface, HILPDA directly inhibits ATGL-mediated lipolysis and downstream mitochondrial FA oxidation, as well as PPARα activation.[18,42] In hypoxia, HILPDA-mediated accumulation of intracellular TG-LDs was shown to be a major mechanism employed to prevent ROS generation associated with FA oxidation and mitigate apoptotic cell death caused by oxidative stress.[18] Although the existing proof of this concept was mostly based upon studies of colorectal and renal cancer, we reasoned that such a defense mechanism would be even more critical for HCC, especially when it develops in a lipid-rich NASH context. Several lines of evidence derived from the current study are in support of this hypothesis. First, ablation of HILPDA decreased TG accumulation and increased oxidative stress in both FA-enriched 2D adherent and 3D HCC spheroid culture systems. Compared to the 2D culture exposed to hypoxia, the 3D spheroids better mimic tumor tissue organization and cell-cell contacts. In particular, they recapitulate critical aspects of tumor biology such as the formation of oxygen concentration

gradients with hypoxic regions, especially at the core of the spheroids.[43] Indeed, we found that wild-type 3D spheroids abundantly express HILPDA even under normoxic conditions. As in the hypoxia-treated 2D system, HILPDA was required to sustain the time-dependent gain of viable cell numbers in the 3D spheroids. Growth of the spheroids lacking HILPDA was severely impaired. In the HCC cells of both culture systems, HILDPA appears to promote cell survival more than cell proliferation, and HILPDA deletion consistently triggered caspase-8/caspase-3-dependent apoptosis when the medium was enriched with FAs. Overall, these findings validate HCC spheroids as a robust model for studying HILPDA in a 3D tumor-like structure that naturally develops hypoxic regions.

Lipid peroxidation plays a critical role in oxidative stress-induced cell death, *i.e.* apoptosis and ferroptosis. Results from the current study provide mechanistic explanations for previously reported observations that PUFAs incorporated into membrane phospholipids are especially susceptible to lipid peroxidation. While the liver tissue in NAFLD is overloaded with a mixture of various saturated, monounsaturated and polyunsaturated FAs, polyunsaturated phospholipids were actually shown to be markedly decreased in human HCC.[44] In this regard, our lipidomics data clearly show that hypoxic treatment upregulates both the total TG accumulation and the enrichment of PUFAs, especially linoleic acid in various TG species. This points to activation of a synthetic mechanism that favors the esterification of PUFAs to TGs in hypoxia. Upon removal of HILPDA, which presumably activates lipolysis, there appears to be an increased flux of PUFAs from TGs to various phospholipids such as PE, phosphatidylserine, phosphatidylglycerol and LPE and cardiolipin. By using ^{14}C-labeled linoleic acid as a PUFA tracer, we were able to obtain direct evidence that HILPDA acts to modulate the partitioning of PUFAs between TG-LDs and phospholipids. The data are in strong support of the concept that by diverting PUFAs away from phospholipids to the TG core of LDs, HILPDA could render cellular and organelle membranes less vulnerable to ROS-induced peroxidation and thereby decrease oxidative damage in hypoxic HCC cells. Our finding that HILPDA ablation caused elevated lipid peroxidation along with severe damage to mitochondrial membrane structures, including mitochondrial fragmentation, rupture of mitochondrial membranes and enlargement of mitochondrial cristae, are consistent with the overall protective role of HILPDA in HCC and other cancer cell types. Mitochondria perform biochemical functions essential for metabolic homeostasis and are key regulators of cell death and survival. As a consequence of mitochondrial damage and unabated ROS production, caspase-8- and caspase-3-mediated cell death was increased in HILPDA-ablated cells. Activation of caspase-8 is a critical upstream step in FA-induced apoptosis, resulting in downstream cleavage and activation of caspase-3.[45] While ferroptosis is not a focus of the current study, the increase of ROS-induced lipid peroxidation of PUFA phospholipids and mitochondrial damage observed in *HILPDA*-KO HCC cells, may suggest a co-activation of both apoptosis and ferroptosis. This result agrees with a recent study that identified HILPDA a HIF-2 downstream effector sensitizing renal cell carcinoma cells to ferroptosis.[32] However, in renal cell carcinoma cells, HILPDA was suggested to enhance PUFA enrichment in both TGs and phospholipids. In this setting, it remains unclear how a TG-promoting lipolytic inhibitor would promote specific PUFA incorporation into phospholipids.

Compared to PUFAs, saturated FAs such as palmitic acid are known to directly elicit lipotoxicity and cellular stress. In hepatocytes, *de novo* synthesis of toxic ceramides is controlled by the availability of palmitoyl-CoA derived from palmitic acid. The monounsaturated oleic acid, on the other hand, is a favored substrate for DGAT-catalyzed TG synthesis and a potent inducer of LD accumulation. In addition, oleic acid is well documented for its ability to ameliorate palmitic acid-induced lipotoxicity. Induction of palmitic acid oxidation or its safe esterification into TGs are among the several mechanisms that have been proposed to underlie this protective effect.[46–48] As oxygen insufficiency impedes mitochondrial FA oxidation, it is conceivable that hypoxic cells could become more reliant on the storage of saturated FAs in TG-LDs for survival. We think this creates a perfect context within which HILPDA plays a pivotal role. In hypoxic HCC cells, HILPDA deficiency led to increased release of saturated FAs and maybe monounsaturated FAs from LDs along with a substantial build-up of various ceramide species. Targeted analysis of various intermediate metabolites suggests that increased *de novo* and salvage ceramide synthesis are the responsible mechanisms. Accordingly, the expression of two major ceramide synthases *CERS2* and *CERS6* was found to be upregulated in the HILPDA-KO cells. That the apoptosis induced by HILPDA deficiency could be reversed by its pharmacological inhibition further demonstrates the functional importance of HILPDA in controlling ceramides in HCC cells. Furthermore, ceramides are emerging as tumor suppressor lipids as they trigger a variety of tumor suppressive programs such as apoptosis, autophagy and senescence.[49–51] Notably, ceramides were reported to be markedly reduced in human HCC.[44] Therefore, we speculate that this HILPDA-mediated mechanism could also promote tumorous transformation of healthy hepatocytes within a tissue microenvironment that is characterized by excessive FAs and normoxia/hypoxia cycles.

In both HCC 2D cell culture and 3D epithelial spheroids, HILPDA depletion dramatically compromised cell growth and spheroid formation, suggesting that HILPDA may play an important role during tumorigenesis *in vivo*. Indeed, we validated the oncogenic potential of HILPDA in the context of Western diet- and CCl_4-induced HCC using mice with hepatocyte-specific *Hilpda* knockout. In our newly developed experimental mouse model, deletion of Hilpda significantly reduced liver weight and alleviated hepatic steatosis and ballooning, though without incurring gross changes in liver enzymes, inflammation or fibrosis. Some of the most notable differences are decreased total nodule count, increased FA oxidation-associated oxidative stress and increased iron storage in *Hilpda*$^{\Delta Hep}$ livers. Despite data obtained from various models that indicated a role for ROS promotion in driving tumor development, no beneficial effect of antioxidants has been detected in cancer prevention studies.[52] On the other hand, additional work has shown that activation of antioxidant defense pathways may instead enhance carcinogenesis.[53] We speculate that this is especially true with NASH-driven HCC, wherein cells are constantly exposed to excessive amounts of exogenous lipids and thus inherently carry a high burden of oxidative stress. The viability of these cells in the harsh NASH liver microenvironment likely depends on the efficient storage of exogenously acquired FAs in TGs and the HILPDA-mediated inhibition of TG breakdown. Exactly how HILPDA contributes to HCC initiation remains to be determined. Given the well-known tumor-suppressive effects of ceramides, one possibility is

that the tumor-promoting effect of HILPDA, at least in part, is conferred through limiting the amount of saturated FAs available for ceramide synthesis.

In the context of NASH, several immune cell types have been implicated in orchestrating a tumor-prone microenvironment. In particular, a recent study identified enrichment of NAMs with unique molecular markers (*Trem2, Apoe, C1qa*) as a key feature of the immune microenvironment of NASH-driven HCC.[27] The fact that Hilpda depletion caused a decreased abundance of NAMs demonstrates an extrinsic role of hepatocyte HILPDA in shaping NASH livers towards a tumor-prone microenvironment. The NAMs appear to exert tumor-promoting activities in NASH, in part by modulating T-cell function.[27] Emerging evidence has linked CD8+ T cell exhaustion to cancer cell evasion of immune surveillance.[54] In this regard, Hilpda deficiency led to increased enrichment of molecular signatures and pathways associated with effector T cell activation and function, conceivably downregulating T cell exhaustion. Furthermore, Hilpda deficiency appeared to alter the liver metabolome landscape, resulting in enrichment of metabolic pathways associated with effector T cell differentiation, proliferation and bioenergetics. As recently reported, such pathways promoted anti-tumor T cell responses.[55–57] Given that induction of NAMs and exhaustion of T cells both occur before any noticeable tumors develop in the NASH liver, our findings raise the possibility that the metabolic remodeling mediated by HILPDA in hepatocytes promotes creation of an immuno-conducive microenvironment prone to liver tumorigenesis.

In conclusion, the current study provides novel evidence that HILPDA acts as an oncometabolic factor in NASH-driven HCC. Our findings unravel mechanistic links between lipolytic control by HILPDA and intracellular FA flux to downstream mitochondrial FA oxidation, ceramide production and lipid peroxidation in HCC cells. Functionally, HILPDA not only promotes survival and growth of HCC cells, but also is critically involved in shaping the liver immune microenvironment and hepatotumorigenesis during NASH. The ability of HILPDA to exert effects on multiple aspects of NASH-driven HCC strongly suggests that identification of future therapeutic strategies targeting HILPDA, in synergy with existing radiotherapy or immunotherapy, might be worth pursuing to potentiate the effectiveness of treatments for NASH-driven HCC.

Supplementary Material

Refer to Web version on PubMed Central for supplementary material.

Acknowledgements

We would like to thank Dr. Harmeet Malhi, Dr. Nicholas LaRusso, Dr. Gregory Gores, Dr. Mark McNiven and Dr. Sumera Ilyas of the Mayo Clinic Rochester Division of Gastroenterology and Hepatology and Dr. John Copland III of the Mayo Clinic Florida Department of Cancer Biology for the constructive feedback during experimental design, data interpretation and manuscript preparation. We would like to thank Dr. Petra Hirsova, Dr. Emilien Loeuillard and Qianqian Guo of the Mayo Clinic Rochester Division of Gastroenterology and Hepatology for kindly providing reagents and sharing equipment. We would like to thank Jenny L. Pattengill of the Mayo Clinic Histology Core for the help with tissue sample sectioning and staining. We would like to thank Trace A. Christensen, Scott I. Gamb and Duane M. Deal of the Mayo Clinic Microscopy and Cell Analysis Core for assistance and guidance with the electron and confocal microscopes. We would like to thank Dr. Lisa Boardman, Donna Felmlee-Devine, Danielle Scherb, Charyl M. Dutton Gibbs, Eugene Krueger of the Mayo Clinic Center for Cell Signaling in Gastroenterology for the help with IRB request, human specimens' procurement, microscopy

equipment, infrastructure and resources needed for this study. We would like to thank Vernadette A. Simon and Fariborz Rakhshan Rohakhtar of the Mayo Clinic Genomics Core for the help with RNA isolation, library preparation and scRNA-sequencing. We would like to thank RaVuth Keo of the Mayo Clinic Pathology Research Core for the assistance with tissue sections and processing for spatial transcriptomics, Colleen Forster of the University of Minnesota Histology and Research Laboratory for guidance with tissue deparaffinization and staining, Grant Barthel of the University of Minnesota Imaging Center for performing Visium gene expression slide imaging, Fernanda Rodriguez and John Garbe of the University of Minnesota Genomics Center for spatial library preparation and transcriptome sequencing.

Financial support

Research reported in this publication was supported by the National Institute of Diabetes and Digestive and Kidney Diseases of the National Institutes of Health under Award number P30DK084567, Satter Foundation Award for Liver Cancer Research, Mayo Clinic Center for Biomedical Discovery Pilot Award and T32 in Diabetes and Metabolism Training under Award number DK07352 to DP; by the Department of Defense under Award number W81XWH-20-1-0903 to JL; and by a Mayo Clinic Cancer Center and Center for Biomedical Discovery Team Award to GLR and JL. The Functional Lipidomics Core at Barshop Institute for Longevity and Aging Studies is partially supported by the National Institute on Aging grants P30 AG013319 and P30 AG044271.

Data availability statement

The data that support the findings of this study are available from the corresponding author, Davide Povero or Jun Liu, upon reasonable request.

Abbreviations

FA	Free fatty acids
IHC	Immunohistochemistry
PA	Palmitic acid
OA	Oleic acid
LA	Linoleic acid
NAFLD	Nonalcoholic fatty liver disease
NASH	Nonalcoholic steatohepatitis
HCC	Hepatocellular carcinoma
HILPDA	Hypoxia-inducible lipid droplet associated protein
NASH-HCC	NASH-driven HCC
HIF	Hypoxia inducible factors
ATGL	Adipose triglycerides lipase
LD	Lipid droplet
TG	Triglycerides
PUFA	Polyunsaturated fatty acid
PL	Phospholipids

WT	Wild-type
KO	Knockout
KD	Knockdown
FFPE	Formalin-fixed paraffin-embedded
BSA	Bovine serum albumin
ALT	Alanine aminotransferase
AST	Aspartate aminotransferase
PE	Phosphatidylethanolamine
PS	Phosphatidylserine
PG	Phosphatidylglycerol
LPE	Lysophosphatidylethanolamine
PC	Phosphatidylcholine
UMAP	Uniform manifold approximation and projection
DN	Dysplastic nodule
aLP	Adjacent liver parenchyma
RT-qPCR	Real-time quantitative polymerase chain reaction
LAM	Lipid-associated macrophages
HSC	Hepatic stellate cells
EC	Endothelial cells
SPTLC1	Palmitoyltransferase long chain base subunit 1
CERS2/6	Ceramide synthase 2 & 6
Gpc3	Glypican-3
Cpt1	Carnitine palmitoyltransferase 1
Fasn	Fatty acid synthase
Fth1	Ferritin heavy chain 1
Hprt	Hypoxanthine-guanine phosphoribosyltransferase
gRNA	Guide RNA
siRNA	Silencing RNA
ROS	Reactive oxygen species

MCD	Methionine- and choline-deficient diet
IRB	Institutional Review Board
CO_2	Carbon dioxide
O_2	Oxygen
CCl_4	Carbon tetrachloride
WD	Western diet
ACSL5	Acyl-CoA synthetase long chain family member 5
MDA	Malondialdehyde
8OHdG	8-Hydroxyguanosine
H&E	Hematoxylin-Eosin
SEM	Scanning electron microscope

References

[1]. Younossi ZM, Blissett D, Blissett R, Henry L, Stepanova M, Younossi Y, et al. The economic and clinical burden of nonalcoholic fatty liver disease in the United States and Europe. Hepatology 2016;64:1577–1586. [PubMed: 27543837]

[2]. Loomba R, Sanyal AJ. The global NAFLD epidemic. Nat Rev Gastroenterol Hepatol 2013;10:686–690. [PubMed: 24042449]

[3]. Adams LA, Lymp JF, St Sauver J, Sanderson SO, Lindor KD, Feldstein A, et al. The natural history of nonalcoholic fatty liver disease: a population-based cohort study. Gastroenterology 2005;129:113–121. [PubMed: 16012941]

[4]. White DL, Kanwal F, El-Serag HB. Association between nonalcoholic fatty liver disease and risk for hepatocellular cancer, based on systematic review. Clin Gastroenterol Hepatol 2012;10:1342–1359 e1342. [PubMed: 23041539]

[5]. Anstee QM, Reeves HL, Kotsiliti E, Govaere O, Heikenwalder M. From NASH to HCC: current concepts and future challenges. Nat Rev Gastroenterol Hepatol 2019;16:411–428. [PubMed: 31028350]

[6]. Llovet JM, Kelley RK, Villanueva A, Singal AG, Pikarsky E, Roayaie S, et al. Hepatocellular carcinoma. Nat Rev Dis Primers 2021;7:6. [PubMed: 33479224]

[7]. Sung H, Ferlay J, Siegel RL, Laversanne M, Soerjomataram I, Jemal A, et al. Global cancer statistics 2020: GLOBOCAN estimates of incidence and mortality worldwide for 36 cancers in 185 countries. CA Cancer J Clin 2021;71:209–249. [PubMed: 33538338]

[8]. Pinyol R, Torrecilla S, Wang H, Montironi C, Pique-Gili M, Torres-Martin M, et al. Corrigendum to 'Molecular characterisation of hepatocellular carcinoma in patients with non-alcoholic steatohepatitis' [J Hepatol 75 (2021) 865-878]. J Hepatol 2021;75:1515. [PubMed: 34627652]

[9]. Hanahan D, Weinberg RA. Hallmarks of cancer: the next generation. Cell 2011;144:646–674. [PubMed: 21376230]

[10]. Masson N, Ratcliffe PJ. Hypoxia signaling pathways in cancer metabolism: the importance of co-selecting interconnected physiological pathways. Cancer Metab 2014;2:3. [PubMed: 24491179]

[11]. Rankin EB, Giaccia AJ. The role of hypoxia-inducible factors in tumorigenesis. Cell Death Differ 2008;15:678–685. [PubMed: 18259193]

[12]. Wang GL, Semenza GL. Purification and characterization of hypoxia-inducible factor 1. J Biol Chem 1995;270:1230–1237. [PubMed: 7836384]

[13]. Gordan JD, Simon MC. Hypoxia-inducible factors: central regulators of the tumor phenotype. Curr Opin Genet Dev 2007;17:71–77. [PubMed: 17208433]

[14]. Papandreou I, Cairns RA, Fontana L, Lim AL, Denko NC. HIF-1 mediates adaptation to hypoxia by actively downregulating mitochondrial oxygen consumption. Cell Metab 2006;3:187–197. [PubMed: 16517406]

[15]. Semenza GL. Defining the role of hypoxia-inducible factor 1 in cancer biology and therapeutics. Oncogene 2010;29:625–634. [PubMed: 19946328]

[16]. Povero D, Johnson SM, Liu J. Hypoxia, hypoxia-inducible gene 2 (HIG2)/HILPDA, and intracellular lipolysis in cancer. Cancer Lett 2020;493:71–79. [PubMed: 32818550]

[17]. Koizume S, Miyagi Y. Lipid droplets: a key cellular organelle associated with cancer cell survival under normoxia and hypoxia. Int J Mol Sci 2016;17.

[18]. Zhang X, Saarinen AM, Hitosugi T, Wang Z, Wang L, Ho TH, et al. Inhibition of intracellular lipolysis promotes human cancer cell adaptation to hypoxia. Elife 2017;6.

[19]. de la Rosa Rodriguez MA, Deng L, Gemmink A, van Weeghel M, Aoun ML, Warnecke C, et al. Hypoxia-inducible lipid droplet-associated induces DGAT1 and promotes lipid storage in hepatocytes. Mol Metab 2021;47:101168. [PubMed: 33465519]

[20]. Grachan JJ, Kery M, Giaccia AJ, Denko NC, Papandreou I. Lipid droplet storage promotes murine pancreatic tumor growth. Oncol Rep 2021:45.

[21]. VandeKopple MJ, Wu J, Auer EN, Giaccia AJ, Denko NC, Papandreou I. HILPDA regulates lipid metabolism, lipid droplet abundance, and response to microenvironmental stress in solid tumors. Mol Cancer Res 2019;17:2089–2101. [PubMed: 31308147]

[22]. van Dierendonck X, de la Rosa Rodriguez MA, Georgiadi A, Mattijssen F, Dijk W, van Weeghel M, et al. HILPDA uncouples lipid droplet accumulation in adipose tissue macrophages from inflammation and metabolic dysregulation. Cell Rep 2020;30:1811–1822 e1816. [PubMed: 32049012]

[23]. van Dierendonck X, Vrieling F, Smeehuijzen L, Deng L, Boogaard JP, Croes CA, et al. Triglyceride breakdown from lipid droplets regulates the inflammatory response in macrophages. Proc Natl Acad Sci U S A 2022;119:e2114739119. [PubMed: 35302892]

[24]. Gimm T, Wiese M, Teschemacher B, Deggerich A, Schodel J, Knaup KX, et al. Hypoxia-inducible protein 2 is a novel lipid droplet protein and a specific target gene of hypoxia-inducible factor-1. FASEB J 2010;24:4443–4458. [PubMed: 20624928]

[25]. McKeown SR. Defining normoxia, physoxia and hypoxia in tumours-implications for treatment response. Br J Radiol 2014;87:20130676. [PubMed: 24588669]

[26]. DiStefano MT, Danai LV, Roth Flach RJ, Chawla A, Pedersen DJ, Guilherme A, et al. The lipid droplet protein hypoxia-inducible gene 2 promotes hepatic triglyceride deposition by inhibiting lipolysis. The J Biol Chem 2015;290:15175–15184. [PubMed: 25922078]

[27]. Zhang P, Chen Z, Kuang H, Liu T, Zhu J, Zhou L, et al. Neuregulin 4 suppresses NASH-HCC development by restraining tumor-prone liver microenvironment. Cell Metab 2022;34:1359–1376 e1357. [PubMed: 35973424]

[28]. Giraud J, Chalopin D, Blanc JF, Saleh M. Hepatocellular carcinoma immune landscape and the potential of immunotherapies. Front Immunol 2021;12:655697. [PubMed: 33815418]

[29]. Wan S, Kuo N, Kryczek I, Zou W, Welling TH. Myeloid cells in hepatocellular carcinoma. Hepatology 2015;62:1304–1312. [PubMed: 25914264]

[30]. Bensaad K, Favaro E, Lewis CA, Peck B, Lord S, Collins JM, et al. Fatty acid uptake and lipid storage induced by HIF-1alpha contribute to cell growth and survival after hypoxia-reoxygenation. Cell Rep 2014;9:349–365. [PubMed: 25263561]

[31]. Salomao M, Remotti H, Vaughan R, Siegel AB, Lefkowitch JH, Moreira RK. The steatohepatitic variant of hepatocellular carcinoma and its association with underlying steatohepatitis. Hum Pathol 2012;43:737–746. [PubMed: 22018903]

[32]. Zou Y, Palte MJ, Deik AA, Li H, Eaton JK, Wang W, et al. A GPX4-dependent cancer cell state underlies the clear-cell morphology and confers sensitivity to ferroptosis. Nat Commun 2019;10:1617. [PubMed: 30962421]

[33]. Kolesnick R, Fuks Z. Radiation and ceramide-induced apoptosis. Oncogene 2003;22:5897–5906. [PubMed: 12947396]

[34]. Gulbins E, Li PL. Physiological and pathophysiological aspects of ceramide. Am J Physiol Regul Integr Comp Physiol 2006;290:R11–R26. [PubMed: 16352856]

[35]. Kagan VE, Mao G, Qu F, Angeli JP, Doll S, Croix CS, et al. Oxidized arachidonic and adrenic PEs navigate cells to ferroptosis. Nat Chem Biol 2017;13:81–90. [PubMed: 27842066]

[36]. Reinartz A, Ehling J, Leue A, Liedtke C, Schneider U, Kopitz J, et al. Lipid-induced up-regulation of human acyl-CoA synthetase 5 promotes hepatocellular apoptosis. Biochim Biophys Acta 2010;1801:1025–1035. [PubMed: 20470896]

[37]. Tsuchida T, Lee YA, Fujiwara N, Ybanez M, Allen B, Martins S, et al. A simple diet- and chemical-induced murine NASH model with rapid progression of steatohepatitis, fibrosis and liver cancer. J Hepatol 2018;69:385–395. [PubMed: 29572095]

[38]. Kleiner DE, Brunt EM, Van Natta M, Behling C, Contos MJ, Cummings OW, et al. Design and validation of a histological scoring system for nonalcoholic fatty liver disease. Hepatology 2005;41:1313–1321. [PubMed: 15915461]

[39]. Gao J, Aksoy BA, Dogrusoz U, Dresdner G, Gross B, Sumer SO, et al. Integrative analysis of complex cancer genomics and clinical profiles using the cBioPortal. Sci Signal 2013;6:pl1. [PubMed: 23550210]

[40]. Wang G, Zhou H, Gu Z, Gao Q, Shen G. Oct4 promotes cancer cell proliferation and migration and leads to poor prognosis associated with the survivin/STAT3 pathway in hepatocellular carcinoma. Oncol Rep 2018;40:979–987. [PubMed: 29901157]

[41]. Sun C, Sun L, Li Y, Kang X, Zhang S, Liu Y. Sox2 expression predicts poor survival of hepatocellular carcinoma patients and it promotes liver cancer cell invasion by activating Slug. Med Oncol 2013;30:503. [PubMed: 23430442]

[42]. Padmanabha Das KM, Wechselberger L, Liziczai M, De la Rosa Rodriguez M, Grabner GF, Heier C, et al. Hypoxia-inducible lipid droplet-associated protein inhibits adipose triglyceride lipase. J Lipid Res 2018;59:531–541. [PubMed: 29326160]

[43]. Tobias F, Hummon AB. Lipidomic comparison of 2D and 3D colon cancer cell culture models. J Mass Spectrom 2022;57:e4880. [PubMed: 36028991]

[44]. Krautbauer S, Meier EM, Rein-Fischboeck L, Pohl R, Weiss TS, Sigruener A, et al. Ceramide and polyunsaturated phospholipids are strongly reduced in human hepatocellular carcinoma. Biochim Biophys Acta 2016;1861:1767–1774. [PubMed: 27570113]

[45]. Cazanave SC, Mott JL, Bronk SF, Werneburg NW, Fingas CD, Meng XW, et al. Death receptor 5 signaling promotes hepatocyte lipoapoptosis. J Biol Chem 2011;286:39336–39348. [PubMed: 21941003]

[46]. Lim JH, Gerhart-Hines Z, Dominy JE, Lee Y, Kim S, Tabata M, et al. Oleic acid stimulates complete oxidation of fatty acids through protein kinase A-dependent activation of SIRT1-PGC1alpha complex. J Biol Chem 2013;288:7117–7126. [PubMed: 23329830]

[47]. Listenberger LL, Han X, Lewis SE, Cases S, Farese RV Jr, Ory DS, et al. Triglyceride accumulation protects against fatty acid-induced lipotoxicity. Proc Natl Acad Sci U S A 2003;100:3077–3082. [PubMed: 12629214]

[48]. Peng G, Li L, Liu Y, Pu J, Zhang S, Yu J, et al. Oleate blocks palmitate-induced abnormal lipid distribution, endoplasmic reticulum expansion and stress, and insulin resistance in skeletal muscle. Endocrinology 2011;152:2206–2218. [PubMed: 21505048]

[49]. Yabu T, Shiba H, Shibasaki Y, Nakanishi T, Imamura S, Touhata K, et al. Stress-induced ceramide generation and apoptosis via the phosphorylation and activation of nSMase1 by JNK signaling. Cell Death Differ 2015;22:258–273. [PubMed: 25168245]

[50]. Guenther GG, Peralta ER, Rosales KR, Wong SY, Siskind LJ, Edinger AL. Ceramide starves cells to death by downregulating nutrient transporter proteins. Proc Natl Acad Sci U S A 2008;105:17402–17407. [PubMed: 18981422]

[51]. Trayssac M, Clarke CJ, Stith JL, Snider JM, Newen N, Gault CR, et al. Targeting sphingosine kinase 1 (SK1) enhances oncogene-induced senescence through ceramide synthase 2 (CerS2)-mediated generation of very-long-chain ceramides. Cell Death Dis 2021;12:27. [PubMed: 33414460]

[52]. Myung SK, Kim Y, Ju W, Choi HJ, Bae WK. Effects of antioxidant supplements on cancer prevention: meta-analysis of randomized controlled trials. Ann Oncol 2010;21:166–179. [PubMed: 19622597]

[53]. Trachootham D, Alexandre J, Huang P. Targeting cancer cells by ROS-mediated mechanisms: a radical therapeutic approach? Nat Rev Drug Discov 2009;8:579–591. [PubMed: 19478820]

[54]. Hirsova P, Bamidele AO, Wang H, Povero D, Revelo XS. Emerging roles of T cells in the pathogenesis of nonalcoholic steatohepatitis and hepatocellular carcinoma. Front Endocrinol (Lausanne) 2021;12:760860. [PubMed: 34777255]

[55]. St Paul M, Saibil SD, Han S, Israni-Winger K, Lien SC, Laister RC, et al. Coenzyme A fuels T cell anti-tumor immunity. Cell Metab 2021;33:2415–2427 e2416. [PubMed: 34879240]

[56]. Siska PJ, Rathmell JC. T cell metabolic fitness in antitumor immunity. Trends Immunol 2015;36:257–264. [PubMed: 25773310]

[57]. Bargiela D, Cunha PP, Velica P, Foskolou IP, Barbieri L, Rundqvist H, et al. Vitamin B6 metabolism determines T cell anti-tumor responses. Front Immunol 2022;13:837669. [PubMed: 35251031]

Highlights

- Hypoxia-mediated HILPDA expression is upregulated and associated with poor survival in HCC.
- HILPDA activation protects HCC cells from cell death under lipid-rich and hypoxic conditions.
- HILPDA deletion dysregulates lipid homeostasis, resulting in ceramide accumulation and enrichment of PUFA in membrane phospholipids.
- Lipid dysregulation resulting from HILPDA deletion leads to apoptosis, lipid peroxidation and mitochondrial damage.
- *In vivo* hepatocyte-specific HILPDA knockout ameliorates steatosis and plays a tumor suppressive role.

Impact and implications

Non-alcoholic steatohepatitis (NASH, chronic metabolic liver disease caused by buildup of fat, inflammation and damage in the liver) is emerging as the leading risk factor and the fastest growing cause of hepatocellular carcinoma (HCC), the most common form of liver cancer. While curative therapeutic options exist for HCC, it frequently presents at a late stage when such options are no longer effective and only systemic therapies are available. However, systemic therapies are still associated with poor efficacy and some side effects. In addition, no approved drugs are available for NASH. Therefore, understanding the underlying metabolic alterations occurring during NASH-driven HCC is key to identifying new cancer treatments that target the unique metabolic needs of cancer cells.

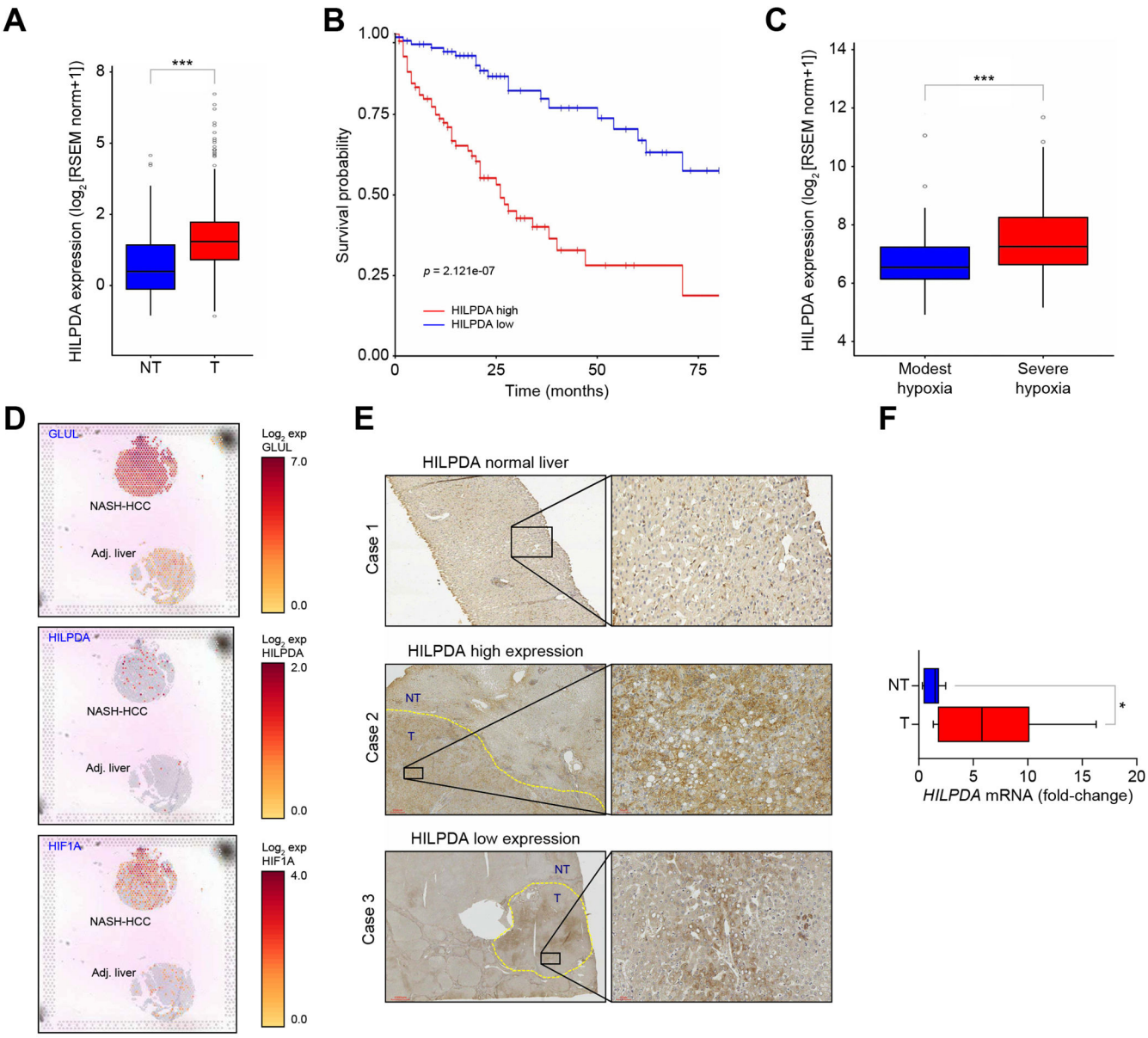

Fig. 1. HILPDA is upregulated in human HCC and NASH-driven HCC.

(A) Bioinformatics analysis of HILPDA expression in human HCC tumor tissue and non-tumor tissues using TCGA's LIHC cohort from cBioPortal and UCSC Xena browser. (B) Kaplan-Meier curve of survival of patients with HCC and high- *vs.* low-expression levels of HILPDA, as determined by TCGA data sets. (C) Hypoxia boxplot correlating *HILPDA* mRNA expression with hypoxia levels (moderate or severe) as determined using the Gene Ontology human response to hypoxia genes (n = 330). (D) 10X Genomics spatial gene distribution of HCC marker *GLUL*, *HILPDA* and *HIF1A* in human NASH-driven HCC tissue and paired adjacent non-cancerous tissue. (E) IHC analysis of HILPDA expression in 8 HCC samples and 4 normal livers. Representative images are shown. (F) RT-qPCR of *HILPDA* mRNA expression in human HCC tumor tissue and non-tumor tissues. 18S was used as a housekeeping gene. Data are presented as mean±SD. (A, C, F) Paired

two-tailed Student's *t* tests were used. Kaplan-Meier survival curve and the log-rank test were used. *p <0.05; **p <0.01; ***p <0.001; ****p <0.0001. GLUL, Glutamine Synthethase; HCC, Hepatocellular carcinoma; HIF1A, Hypoxia inducible factor 1alpha; HILPDA, Hypoxia-inducible lipid droplet associated protein; TCGA-LIHC, Cancer Genome Atlas Liver Hepatocellular Carcinoma; RT-qPCR, quantitative real-time polymerase chain reaction.

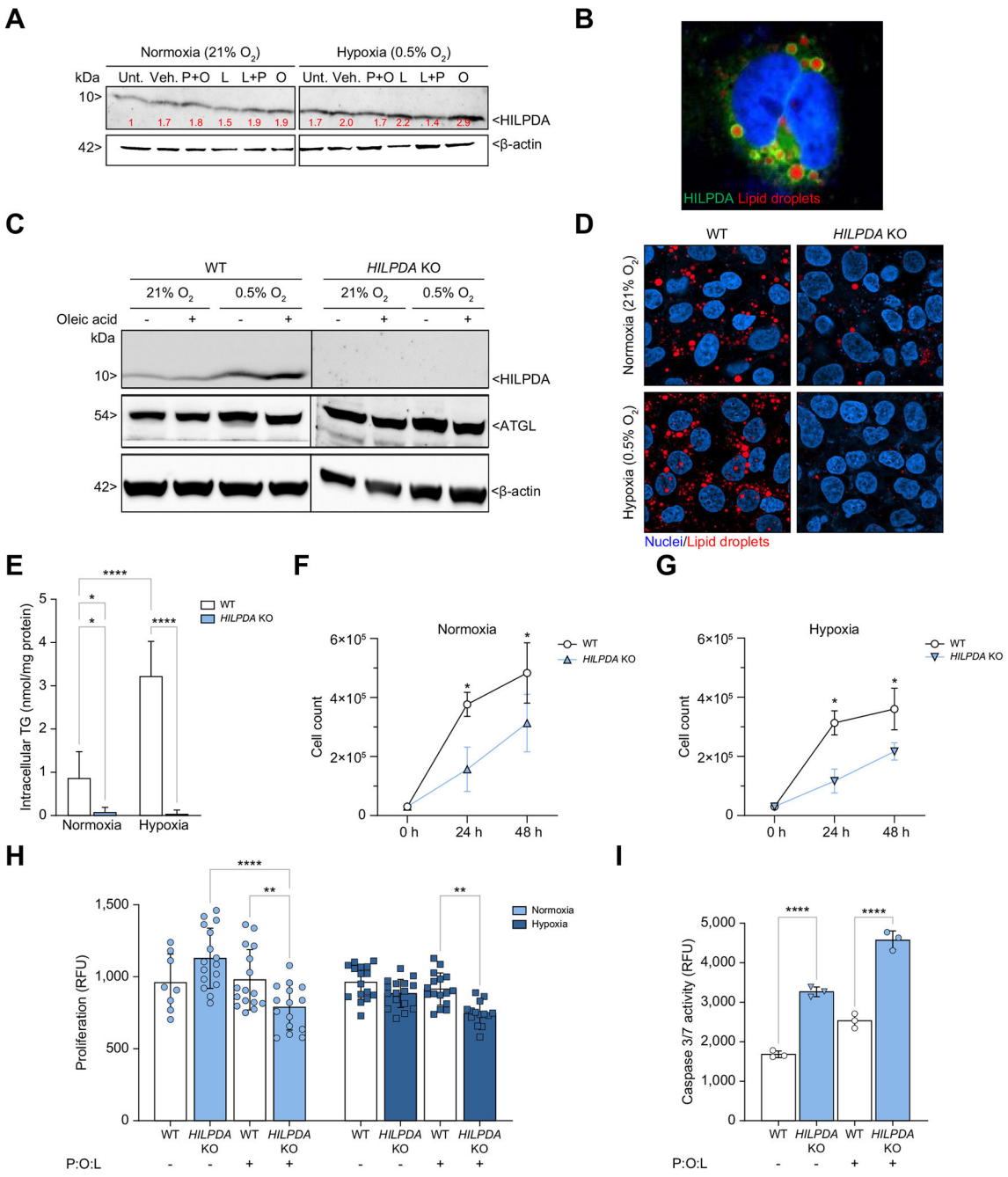

Fig. 2. HILPDA promotes HCC cell growth and survival.

(A) Western blot analysis of HILPDA in Huh7 cells exposed to normoxia (21% O_2) or hypoxia (0.5% O_2) and with or without exogenous free FAs (150 μM) for 16 h. Relative protein quantification is indicated in red as fold-change for each experimental condition. β-actin was used as loading control. (B) Immunofluorescent analysis of HILPDA which localizes around LDs (red) in Huh7 cells exposed to hypoxia and oleic acid (150 μM) for 16 h. (C) Western blot analysis of HILPDA and ATGL in WT and HILPDA KO Huh7 cells exposed to normoxia (21% O_2) or hypoxia (0.5% O_2) and with or without OA (150 μM)

for 16 h. β-actin was used as loading control. (D) Fluorescent-based imaging of neutral lipids stored in LDs (red) and identified using LipidTOX in WT and HILPDA KO Huh7 cells exposed to normoxia (21% O_2) or hypoxia (0.5% O_2) and with or without OA (150 μM) for 16 h. (E) Intracellular TG level (nmol/mg proteins) in WT and HILPDA KO Huh7 cells exposed to normoxia (21% O_2) or hypoxia (0.5% O_2) and with or without OA (150 μM) for 16 h. (F, G) Cell viability analysis of WT and HILPDA KO Huh7 cells exposed to normoxia (21% O_2) or hypoxia (0.5% O_2) for up to 48 h. (H) Proliferation assay in WT and HILPDA KO Huh7 cells exposed to normoxia (21% O_2) or hypoxia (0.5% O_2) and with or without 400 μM of FA mix (palmitic:oleic:linoleic acids) for up to 48 h. (I) Caspase 3/7 activity assay in WT and HILPDA KO Huh7 cells exposed to hypoxia (0.5% O_2) and with or without 400 μM of FA mix (palmitic:oleic:linoleic acids) for 24 h. Data are means±SD. Paired two-tailed Student's t tests were used. (H, I) Nonparametric Kruskal-Wallis ANOVA test was used. *p <0.05; **p <0.01; ***p <0.001; ****p <0.0001. FA, fatty acid; KO, knockout; L, linoleic acid; O, oleic acid; P, palmitic acid; Veh, vehicle (0.5% FA-free BSA); WT, wild-type.

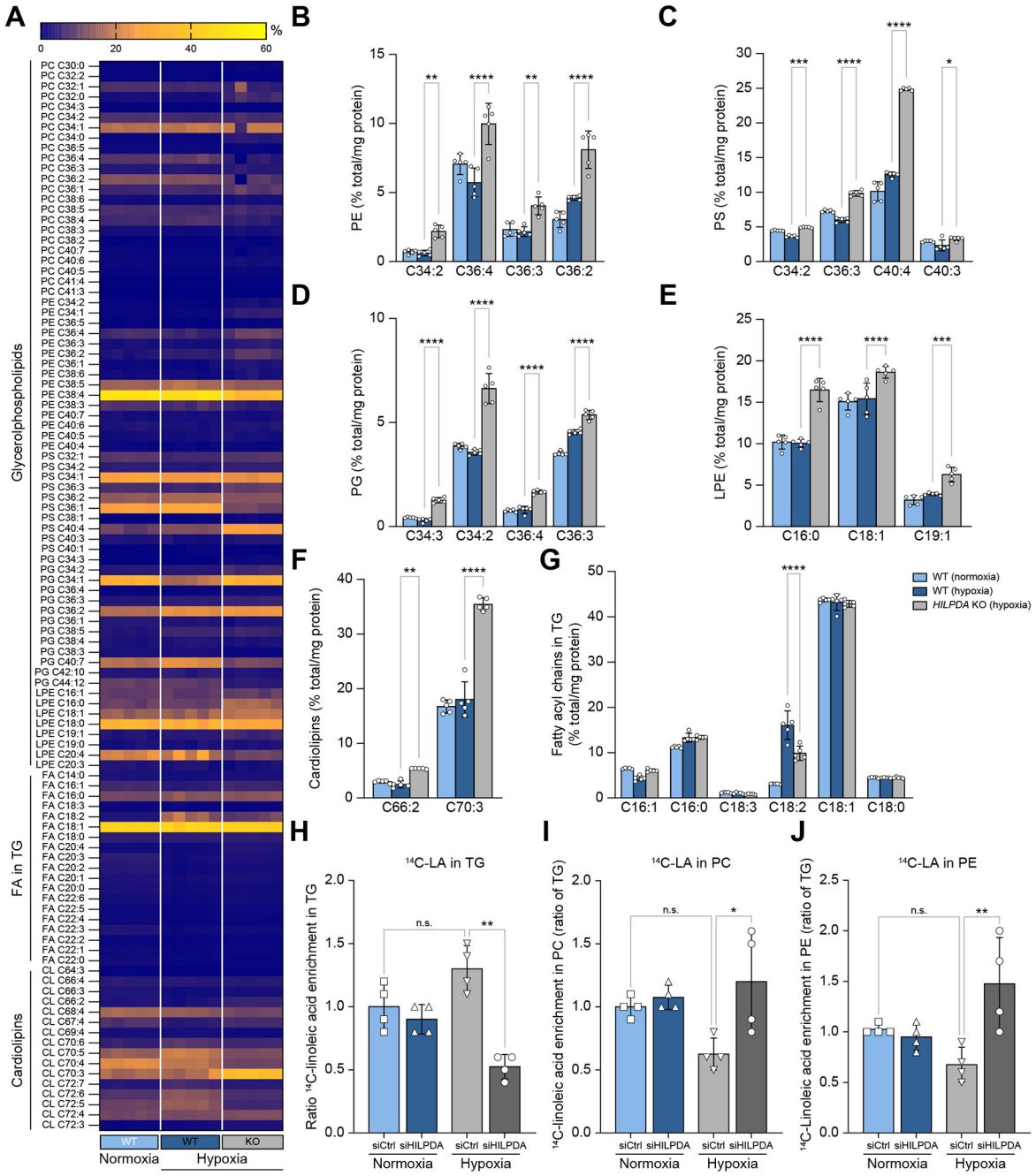

Fig. 3. HILPDA deletion disrupts lipid homeostasis and increases PUFA-enrichment in membrane phospholipids.

(A) Heatmap of lipid species in WT and HILPDA knockout Huh7 cells exposed to normoxia (21% O_2) or hypoxia (0.5% O_2) and 200 μM oleic acid for 24 h, analyzed by multidimensional mass spectrometry (MDMS)-based shotgun lipidomics (MDMS-SL). Values reported as percentage of total lipids in each species. (B–G) Levels of representative individual lipid species with polyunsaturated fatty acyl chains (C18:2, C18:3, C20:4) in WT and HILPDA KO Huh7 cells exposed to normoxia (21% O_2) or hypoxia (0.5% O_2) and 200 μM oleic acid for 24 h. (H–J) Levels of ^{14}C-linoleic acid enrichment ratios

in triglycerides, phosphatidylcholine and phosphatidylethanolamine in Huh7 cells treated with HILPDA siRNA (siHILPDA) or control siRNA (siControl) and exposed to normoxia (21% O_2) or hypoxia (0.5% O_2), 0.2 μCi/ml linoleic acid [1-^{14}C] and 150 μM of cold linoleic acid for 24 h. Data are presented as mean±SD. (B-J) Non-parametric Kruskal-Wallis ANOVA test was used. *p <0.05; **p <0.01; ***p <0.001; ****p <0.0001. FA, fatty acid; KO, knockout; LPE, lysophosphatidylethanolamine; PC, phosphatidylcholine; PE, phosphatidylethanolamine; PG, phosphatidylglycerol; PS, phosphatidylserine; WT, wild-type.

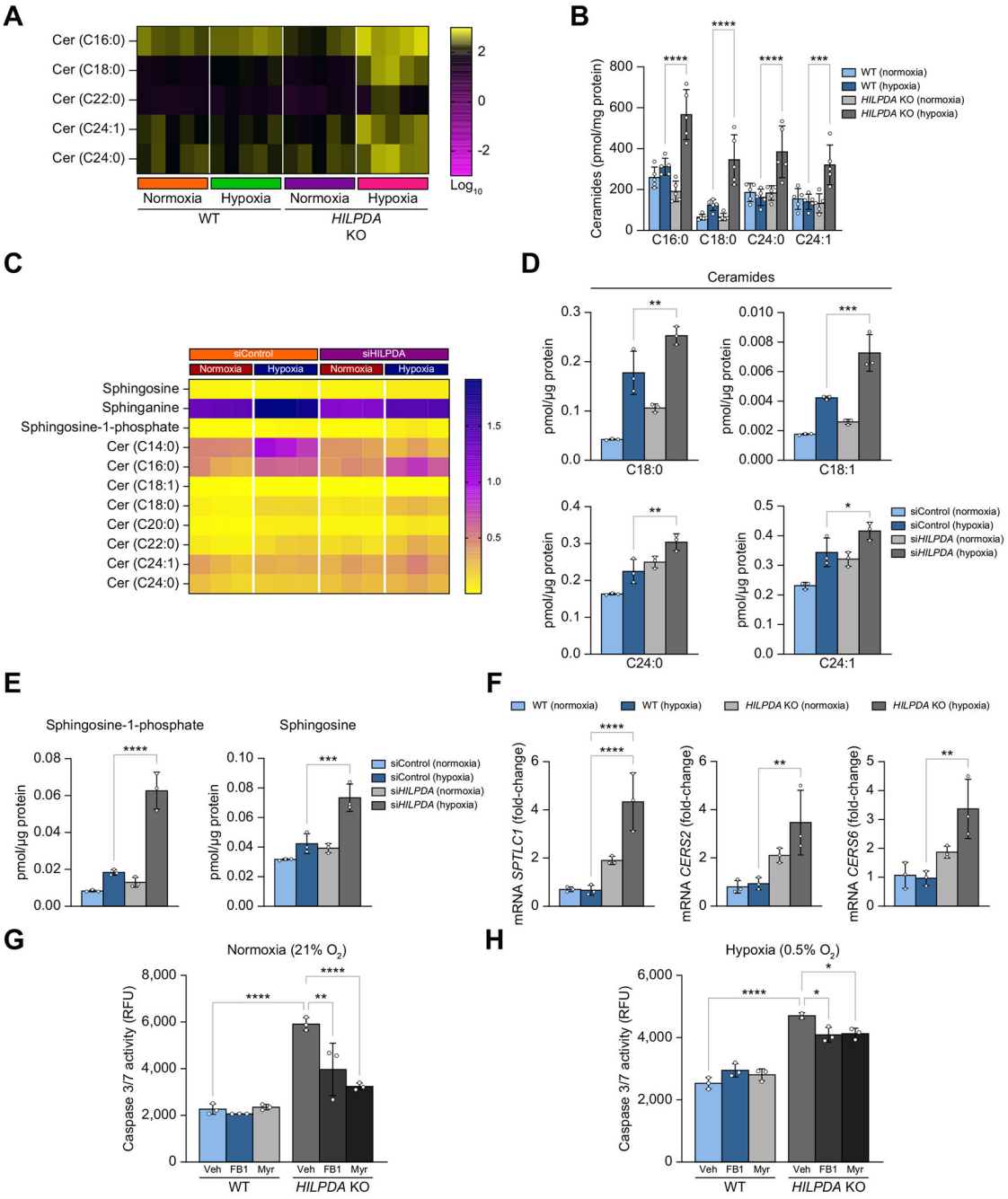

Fig. 4. HILPDA deficiency disrupts sphingolipid homeostasis leading to apoptosis of HCC cells.

(A) Heatmap of ceramide species in WT and HILPDA KO Huh7 cells exposed to normoxia (21% O_2) or hypoxia (0.5% O_2) and 200 μM oleic acid for 24 h, analyzed by multidimensional mass spectrometry-based shotgun lipidomics. (B) Levels of representative individual ceramide species in WT and HILPDA KO Huh7 cells exposed to normoxia (21% O_2) or hypoxia (0.5% O_2) and 200 μM oleic acid for 24 h. (C) Heatmap of sphingolipid species in Huh7 cells treated with HILPDA siRNA (siHILPDA) or control siRNA (siControl) and exposed to normoxia (21% O_2) or hypoxia (0.5% O_2) and 200 μM oleic

acid for 24 h, analyzed by liquid chromatography tandem mass spectrometry. (D, E) Levels of representative individual sphingolipid species in in Huh7 cells treated with HILPDA siRNA (siHILPDA) or control siRNA (siControl) and exposed to normoxia (21% O_2) or hypoxia (0.5% O_2) and 200 μM oleic acid for 24 h. (F) RT-qPCR analyses of *SPTLC1*, *CERS2* and *CERS6* in WT and HILPDA KO Huh7 cells exposed to normoxia (21% O_2) or hypoxia (0.5% O_2) and 200 μM oleic acid for 24 h. 18S was used as a housekeeping gene. (G, H) Caspase 3/7 activity assay in WT and HILPDA KO Huh7 cells exposed to normoxia (21% O_2) or hypoxia (0.5% O_2) and 400 μM FA mix (palmitic:oleic:linoleic acids) for 24 h with or without 10 μM of FB1, 10 μM of Myr or vehicle control (0.1% DMSO). Data are presented as mean ± SD. (B, D–H) Non-parametric Kruskal-Wallis ANOVA test was used. *p <0.05; **p <0.01; ***p <0.001; ****p <0.0001. Cer, ceramide; KO, knockout; WT, wild-type.

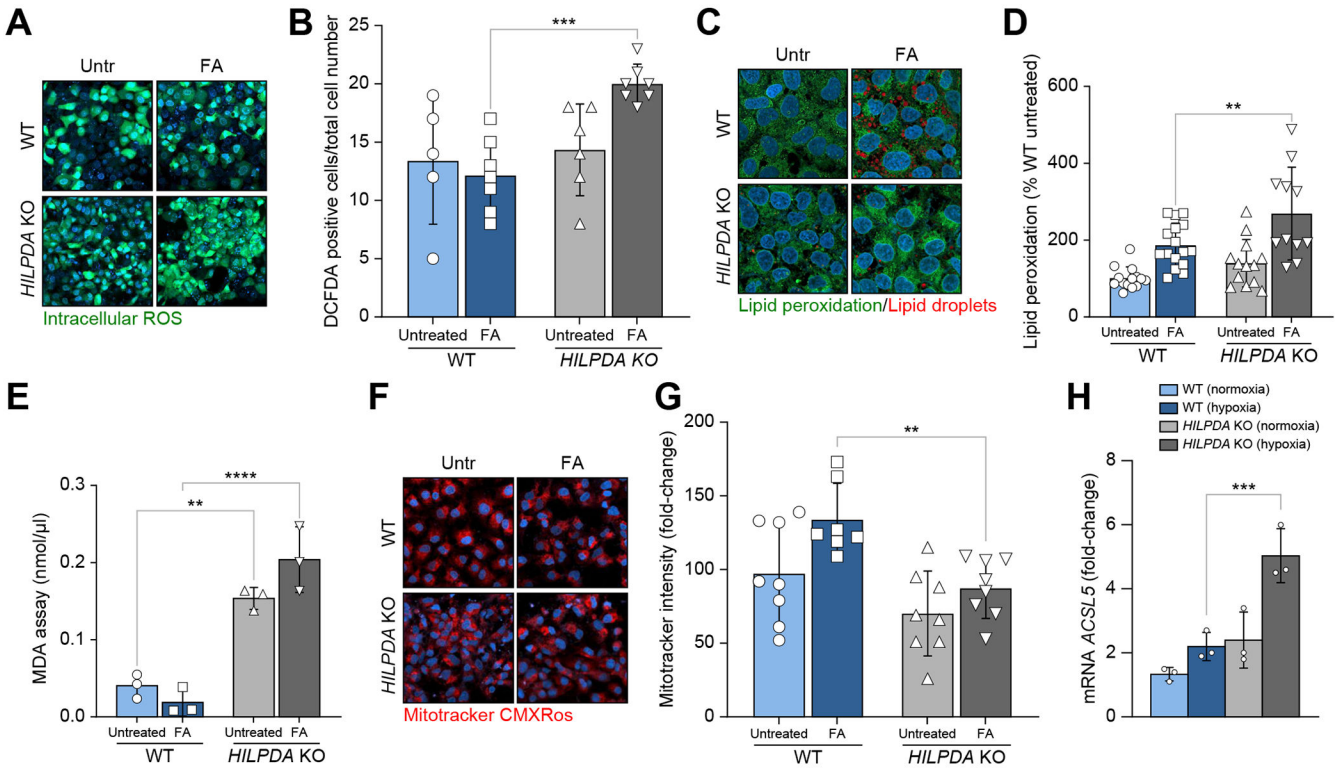

Fig. 5. HILPDA deletion leads to enrichment of PUFAs in cell membranes and leads to oxidative stress, lipid peroxidation and mitochondrial dysfunction.

(A) Representative fluorescence-based images and (B) quantitation of intracellular ROS levels detected by DCFDA assay in WT and HILPDA KO Huh7 cells exposed to normoxia (21% O_2) or hypoxia (0.5% O_2) and 300 µM FA mix (palmitic:oleic:linoleic acids) for 72 h. (C) Representative fluorescence-based images and (D) quantitation of membrane lipid peroxidation levels detected by linoleamide alkyne assay in WT and HILPDA KO Huh7 cells exposed to normoxia (21% O_2) or hypoxia (0.5% O_2) and 300 µM FA mix (palmitic:oleic:linoleic acids) for 72 h. (E) Intracellular levels of MDA in WT and HILPDA KO Huh7 cells exposed to normoxia (21% O_2) or hypoxia (0.5% O_2) and 300 µM FA mix (palmitic:oleic:linoleic acids) for 72 h. (F) Representative fluorescence-based images and (G) quantitation of mitochondrial membrane potential using MitoTracker Red CMXRos in WT and HILPDA KO Huh7 cells exposed to normoxia (21% O_2) or hypoxia (0.5% O_2) and 300 µM FA mix (palmitic:oleic:linoleic acids) for 72 h. (H) RT-qPCR analysis of *ACSL5* mRNA expression in WT and HILPDA KO Huh7 cells exposed to normoxia (21% O_2) or hypoxia (0.5% O_2) and 300 µM FA mix (palmitic:oleic:linoleic acids) for 24 h. Data are presented as mean±SD. (B, D, E, G, H) Non-parametric Kruskal-Wallis ANOVA test was used. *p <0.05; **p <0.01; ***p <0.001; ****p <0.0001. KO, knockout; MDA, malondialdehyde; WT, wild-type.

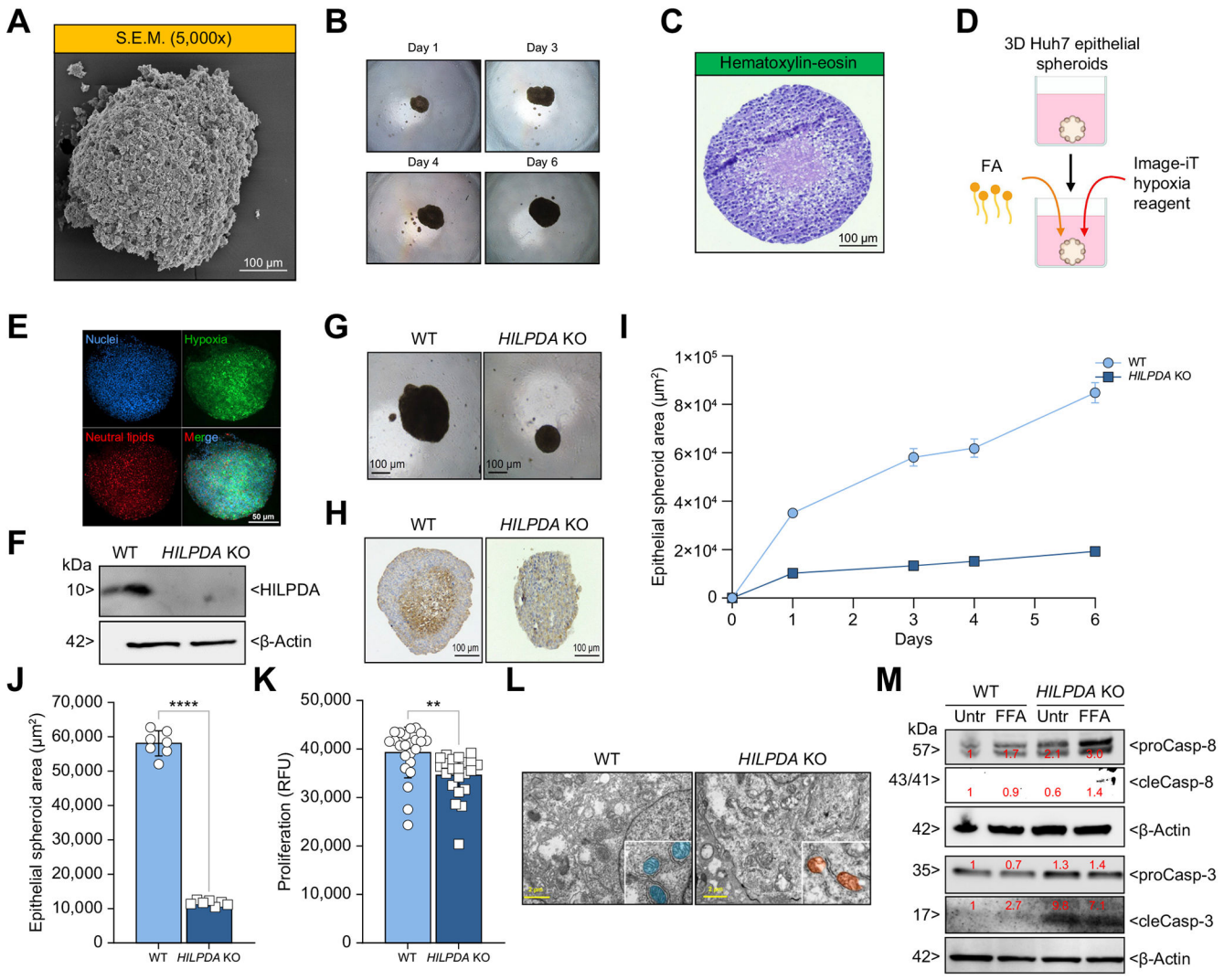

Fig. 6. HILPDA depletion arrests 3D HCC spheroids formation, size growth and survival.

(A) Scanning electron microscope imaging of 3D Huh7 epithelial spheroid. (B) Brightfield images of 3D Huh7 epithelial spheroid over 6 days in culture. (C) H&E staining of longitudinal section of formalin-fixed paraffin-embedded 3D Huh7 epithelial spheroid. (D) Procedural scheme of 3D Huh7 epithelial spheroid treatment with 400 µM of FA mix (palmitic:oleic:linoleic acids) and Image-iT hypoxia fluorescence-based reagent. (E) Fluorescence-based imaging of 3D Huh7 epithelial spheroid treated with 400 µM of FA mix (palmitic:oleic:linoleic acids) for 48 h. Hypoxic regions were detected with Image-iT hypoxia reagent, neutral lipids (red) with LipidTOX and cell nuclei (blue) with Hoechst33342 and imaged with Zeiss LSM980 with Airyscan 2. (F) Western blot analysis of HILPDA in wild-type (WT) and HILPDA KO 3D Huh7 epithelial spheroids. β-actin was used as loading control. (G) Brightfield images of WT and HILPDA KO 3D Huh7 epithelial spheroids. (H) IHC for HILPDA in wild-type (WT) and HILPDA KO 3D Huh7 epithelial spheroids. (I) Spheroid area (µm^2) of WT and HILPDA KO 3D Huh7 epithelial spheroids over 6 days in culture. (J) Spheroid area (µm^2) of WT and HILPDA KO 3D

Huh7 epithelial spheroids after 2 weeks in culture. (K) Proliferation assay of WT and HILPDA KO 3D Huh7 epithelial spheroids after 72 h. (L) Transmission electron microscopy images of WT and HILPDA KO 3D Huh7 spheroid sections, where mitochondria have been pseudocolored. (M) Western blot analyses of pro-/active caspase-8 and pro-/active caspase3 in WT and HILPDA KO 3D Huh7 spheroids with or without 400 μM of FA mix (palmitic:oleic:linoleic acids). Relative protein quantification is indicated in red as fold-change for each experimental condition. β-actin was used as loading control. Data are means±SD. (J, K) Paired two-tailed Student's *t* tests were used. *p <0.05; **p <0.01; ***p <0.001; ****p <0.0001. KO, knockout; WT, wild-type.

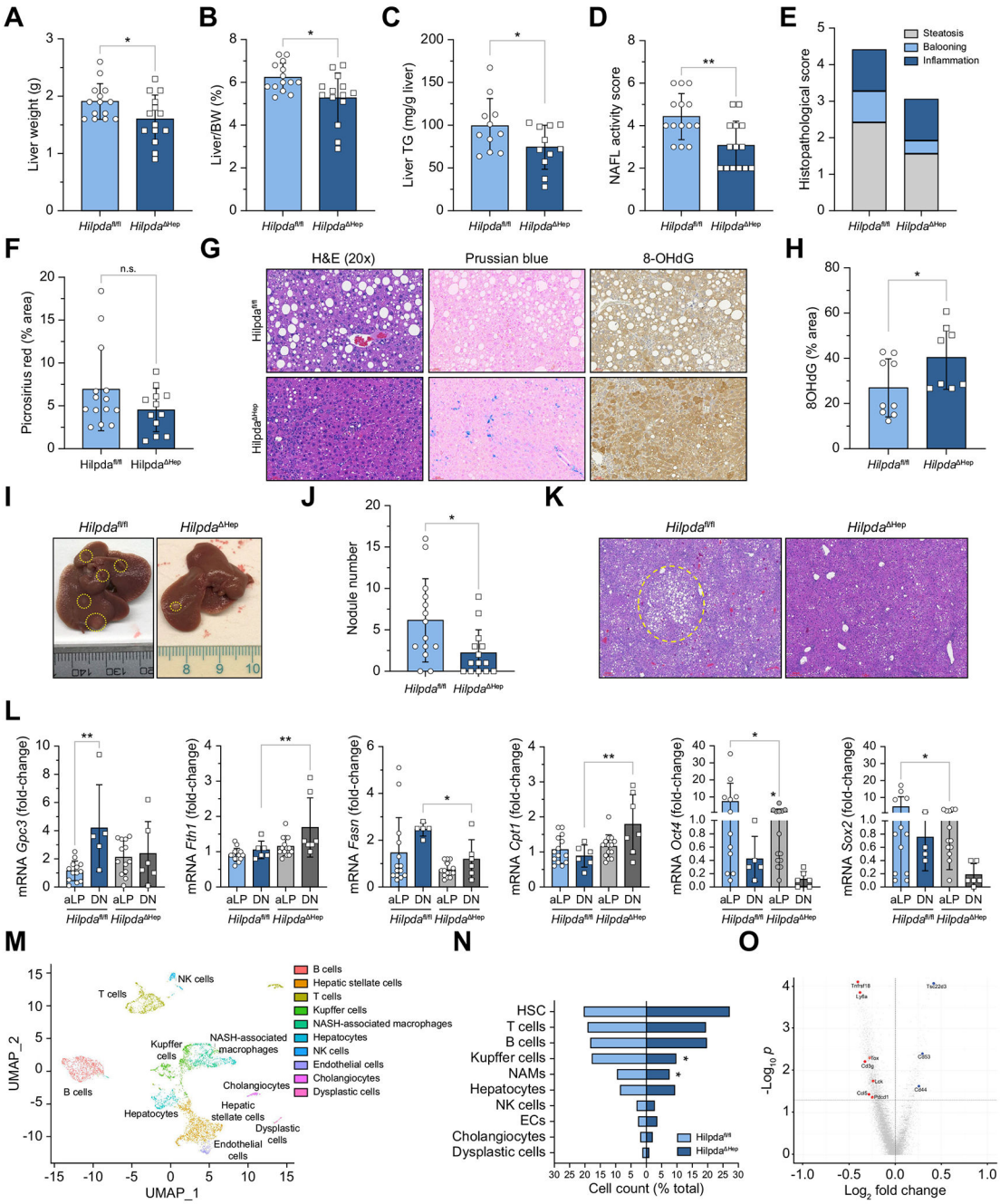

Fig. 7. Hepatocyte-specific Hilpda knockout ameliorates liver steatosis and impedes NASH-driven HCC formation *in vivo*.

Hepatocyte-specific Hilpda knockout (*Hilpda*$^{\Delta Hep}$) and Hilpda-floxed control (*Hilpda*$^{fl/fl}$) C57/B6 mice (n = 14 mice/group) were fed a Western diet plus sugar water and injected weekly with CCl_4 intraperitoneally for 24 weeks. (A) Liver weight. (B) Liver/BW ratio. (C) Levels of hepatic triglycerides (mg/g liver). (D) NAFLD activity score and (E) individual scores for steatosis, ballooning, and inflammation in liver samples of indicated experimental groups. (F) Quantitation of picrosirius red staining for liver fibrosis in the indicated experimental groups. (G) H&E, Prussian blue staining (iron accumulation) and

IHC for 8-OHdG (oxidative stress marker) in liver tissue for indicated experimental groups. (H) Quantitation of hepatic levels of 8-OHdG for indicated experimental groups. (I) Gross images of livers highlighting dysplastic nodules (yellow circles) in the indicated experimental groups. (J) Number of dysplastic nodules in each of the indicated experimental group.[22] (K) Representative H&E staining of liver tissues for the indicated experimental groups. (L) RT-qPCR analyses of *Gpc3*, *Cpt1*, *Fasn*, *Fth1*, *Oct4* and *Sox2* mRNA expression in adjacent liver parenchyma[38] and dysplastic nodules[39] harvested from the indicated experimental groups. Hprt was used as a housekeeping gene. (M) UMAP plots of liver cell clusters identified by single-cell RNA-seq analysis in both experimental groups (n = 2 mice/group). (N) Relative cell count normalized on total count of each liver cell cluster in the indicated experimental groups. (O) Volcano plot of differentially expressed genes in $Hilpda^{\Delta Hep}$ *vs.* $Hilpda^{fl/fl}$ T cells identified by single-cell RNA-seq analysis (n = 2 mice/group). Data are presented as mean ± SD. (A–D, F, G, J) Paired two-tailed Student's *t* tests were used. (L) Non-parametric Kruskal-Wallis ANOVA test was used. (N) Two-proportions z-test was used. *p <0.05; **p <0.01; ***p <0.001; ****p <0.0001. BW, body weight; NAFLD, non-alcoholic fatty liver disease; NASH, non-alcoholic steatohepatitis; NK, natural killer; UMAP, uniform manifold approximation and projection.

Table 1.

Baseline characteristics of the study population.

Baseline characteristics	
Demographics	
Age, years	68 (62–75)
Male	75% (6)
BMI, kg/m^2	36 (26–47)
Liver tests	
AST	268 (79–663)
ALT	246 (69–492)
Histology	
Histology confirmation of HCC	100%
Median tumor size (cm)	5.7 (1.6–11)
Tumor focality (solitary)	87.5%
Cirrhosis	62.5%
Fibrosis stage	
F0–2	25%
F3	25%
F3–4	25%
F4	25%
Grading	
G1	–
G2	87.5%
G2-3	12.5%
Primary therapy	
Resection	100%
Comorbidities	
Type 2 diabetes	75%
Hypertension	87.5%
Atherosclerosis	37.5%
Morbid obesity	37.5%

ALT, alanine aminotransferase; AST, aspartate aminotransferase; HCC, hepatocellular carcinoma. A cohort of eight individuals with histopathologically proven non-alcoholic steatohepatitis-driven HCC was included in the study. Tumor paired with adjacent non-tumor tissue samples were used for analyses. All data are presented as the median (interquartile range) or percentage.